

RESEARCH ARTICLE

Evolution of the northern Turkana Depression (East African Rift System, Kenya) during the Cenozoic rifting: New insights from the Ekitale Basin (28–25.5 Ma)

Théa Ragon^{1,2}  | Alexis Nutz^{1,3,4} | Mathieu Schuster¹ | Jean-Francois Ghienne¹ |
Gilles Ruffet⁵ | Jean-Loup Rubino⁶

¹Université de Strasbourg, CNRS, Institut de Physique du Globe de Strasbourg, UMR 7516, Strasbourg, France

²Université Côte d'Azur, CNRS, Observatoire de la Côte d'Azur, IRD, Géoazur, Valbonne, France

³Department of Geoscience, Aarhus University, Aarhus, Denmark

⁴Aix-Marseille Université, CNRS, IRD, Collège de France, Centre Européen de Recherche et d'Enseignement des Géosciences de l'Environnement, Aix en Provence, France

⁵Géosciences Rennes, CNRS (CNRS/INSU) UMR 6118 and Université de Rennes 1, Géosciences Rennes, Rennes, France

⁶Total SA, CSTJF, Pau, France

Correspondence

Théa Ragon, Observatoire de la Côte d'Azur, IRD, Géoazur, Université Côte d'Azur, CNRS, Valbonne, France.

Email: ragon@geoazur.unice.fr

Funding information

Total, Grant/Award Number: Rift Lake Sedimentology - RiLakS

Handling Editor: M. Patacci

Two sedimentary basins are identified in the Turkana Depression (East African Rift System, Kenya). One of them, the Ekitale Basin, is presented in detail. Located on the western rift shoulder of the northern Turkana Depression, the preserved portion of the Ekitale Basin is 3–5-km wide and bordered by N40°–50° normal faults. These normal faults were inherited from the reactivation of pre-existing basement structures. The Ekitale Basin is filled by the ~75-m-thick Topernawi Formation. The lower portion of the formation provides evidence that the basin was occupied by a lake, bordered by alluvial fans, and into which river-derived turbiditic complexes were deposited. The upper portion is comprised of pyroclastic deposits, originating from volcanic activity, and interbedded with fluvial deposits emplaced during periods of volcanic quiescence. The Ekitale Basin opened just after 28 Ma and was abandoned prior to 25 Ma, placing it after the deposition of the Oligocene Traps (ca. 33.9–27 Ma) and prior to the rift climax (after 14 Ma). This syn-rift basin largely impacts our understanding of the Cenozoic rift evolution in the Turkana Depression. It helps to identify, for the first time, the first pulse of extension of the Cenozoic rifting, revealing a two-step rifting scenario for the northern Turkana Depression. The Ekitale Basin, and analogous syn-rift basins, is believed to have developed from the reactivation of pre-existing structures during a period of extension marked by low differential stress and a low amount of extension.

KEYWORDS

continental rift, early rifting, fan delta, fluvio-lacustrine, Oligocene, Topernawi Formation, turbidites, volcanioclastics

1 | INTRODUCTION

The successive steps in the evolution of a continental rift have been outlined in several analogical and conceptual models (e.g., Cowie, 1998; Cowie, Gupta, & Dawers, 2000; Fossen & Rotevatn, 2016; Gawthorpe & Leeder, 2000; Gupta, Cowie, Dawers, & Underhill, 1998; Whipp, Jackson, Schlische, Withjack, & Gawthorpe, 2016). In these models, the early phase of continental rifting is characterized by the development of kilometre-scale, juxtaposed and isolated

depocenters bordered by normal faults. These faults are oriented perpendicular to the direction of the extension. Subsequently, ongoing extension results in the linkage of these kilometre-scale depocenters and the development of larger half-grabens or grabens (tens of kilometres long and wide) bordered by major normal faults oriented in a similar direction (Ackermann, Schlische, & Withjack, 2001; Cartwright, Trudgill, & Mansfield, 1995; Dawers & Anders, 1995; Gupta et al., 1998; Mansfield & Cartwright, 2001). These two successive phases are summarized in a two-step model of rifting (Prosser, 1993)

referred to as the initiation stage and the rift climax. However, field-based investigations of such rift evolution are rare, particularly for the earliest phases of evolution, highlighting the need for ground-truth validation of these evolutionary models.

Following the pioneering work of Gregory (1896), the East African Rift System (EARS) has been investigated intensively through a combination of field geology and seismic imagery. The morphologies of half-grabens and grabens as well as the location of transfer and relay zones are now well constrained (e.g., Chorowicz, 2005; Macgregor, 2015; Morley, 1999; Morley et al., 1992; Rosendahl, 1987; Simon et al., 2017; Tiercelin & Lezzar, 2002). Nevertheless, unresolved issues remain about the past evolution of the EARS. First, the timing of rift initiation is only partially understood along both the western and the eastern branches of the EARS. Second, early rift evolution is very poorly documented. Third, the successive evolutionary steps of Cenozoic rifting and their genetic relationships with stress evolution remain poorly understood. Finally, although the history of Cenozoic rifting of the EARS is relatively well understood at a continental scale, detailed reconstructions of rifting at the local scale are rare. The latter is particularly true for long-lived active areas such as the Turkana Depression (Figure 1) where syn-rift basins have only been described for the most recent 5 Ma, notably through the investigation of the Plio-Quaternary Omo Group (e.g., Gathogo & Brown, 2006; Harris, Leakey, & Brown, 1988; McDougall & Feibel, 1999; Nutz, Schuster, Boës, & Rubino, 2017; Tiercelin et al., 2010). Earlier events in this area remain scarcely documented.

In this study, we aim to refine our understanding of the EARS history in the northern Turkana Depression through field-based investigations. Two previously unknown basins are identified, allowing to explore in detail the early evolution of the Cenozoic rifting in the area. One of them is not easily reachable and will need further investigation. The other, named Ekitale Basin (Figure 1), is infilled by a ~75-m-thick sediment accumulation that we name the Topernawi Formation (Figure 2). Description of the Ekitale Basin provides a novel vision of regional rift evolution, revealing a two-step Cenozoic rifting scenario for this area. This study aims to (a) characterize the tectono-sedimentary evolution of the Ekitale Basin, (b) reveal the timing of its initiation and abandonment, (c) integrate this basin into the Cenozoic rifting history of the northern Turkana Depression, and (d) discuss controls on the nature of the successive syn-rift basins in the northern Turkana Depression. Building upon geological mapping, cross-sections and the interpretation of sedimentary infill cropping out along river incisions, we propose a synthetic tectono-sedimentary model that illustrates the complete evolution of Cenozoic rifting in the northern Turkana Depression. Our study offers a field-based example of rift initiation and evolution. It also highlights a new phase in the rift evolution that likely develops due to specific stress conditions, either during periods of early rifting or decreased relative extension within a phase of larger scale rifting.

2 | GEOLOGICAL BACKGROUND

2.1 | Regional structural framework

The Turkana Depression, part of the EARS (Figure 1a), corresponds to a 300-km-long and 200-km-wide lowland separating the Main

Ethiopian Rift to the north and the Kenyan Rift to the south (Brune, Corti, & Ranalli, 2017; Dunkelman, Karson, & Rosendahl, 1988; Dunkelman, Rosendahl, & Karson, 1989; Ebinger et al., 2000; Morley et al., 1999; Rosendahl, 1987; Tiercelin et al., 2012; Wescott et al., 1993). The Turkana Depression is composed of several N-S-oriented half-grabens (Figure 1b,c) that developed during several episodes of extension dating from the Upper Eocene/Lower Oligocene to the present (Macgregor, 2015; Morley et al., 1999; Tiercelin & Lezzar, 2002; Vétel & Le Gall, 2006). The area contains three large-scale basement-inherited fault zones, oriented NE-SW and NW-SE (Figure 1b) known as the Buluk, Kataboi, and N'Doto-Karisia fault zones (BFZ, KFZ, and NKFZ, respectively; Vétel, 2005; Vétel & Le Gall, 2006). The NKFZ in particular is thought to have influenced the nucleation and the distribution of basins in the Turkana Depression throughout Cenozoic rifting (Vétel & Le Gall, 2006).

The Turkana Depression is subdivided into two main parts based on structural characteristics. The southern part of the Turkana Depression—the most well-documented area due to oil exploration (Tiercelin, Thuo, Potdevin, & Nalpas, 2012)—consists of five juxtaposed N-S-oriented half-grabens known as the Naipa, Lokichar, Turkwel, Kerio, and South Lake basins (Figure 1b,c). These five basins form an up to 8-km-deep and > 00-km-wide rift system (*sensu* Buck, 1991) characterized by relatively low relief due to the low elevation of the basin shoulders. In this area, Cenozoic rifting is believed to have started *ca.* 35 Ma in the Lokichar Basin (Morley et al., 1999; Vétel & Le Gall, 2006). During the Early Miocene (23–15 Ma), rifting extended farther east with the opening of the Turkwel and Kerio basins (Vétel & Le Gall, 2006). Slightly before 10 Ma, the South Lake Basin was likely already open (Morley et al., 1999; Vétel & Le Gall, 2006).

In contrast, the northern part of the Turkana Depression (Figure 1b), markedly less well known, consists of a single 80-km-wide, >4-km-deep (Abdelfattah et al., 2016) N-S-oriented asymmetric graben known as the North Lake Basin (Figure 1c; Hendrie, Kusznir, Morley, & Ebinger, 1994; Morley et al., 1999; Tiercelin et al., 2004; Vétel & Le Gall, 2006). The North Lake Basin forms a narrow rift (*sensu* Buck, 1991) and is bounded to the west by the N-S-oriented Murua Rith-Lapurr Fault (MRLF, Figure 1b). Eastward of the MRLF, the basin is affected by several minor normal faults followed by a second major fault referred to as the Shore Fault (Nutz et al., 2017), located along the western shore of present-day Lake Turkana (Figure 1b,c). West of the MRLF, the North Lake Basin is bordered by a relatively high-relief shoulder known as the Murua Rith Hills and the Lapurr Range. The opening of the North Lake Basin is generally thought to have been initiated between the Upper Miocene (9 Ma) and Middle Pliocene (4.2 Ma) (Feibel, 2011; Morley et al., 1999; Vétel & Le Gall, 2006).

2.2 | Regional stratigraphic framework

In the Turkana Depression, the basement is composed of metamorphic Proterozoic rocks (Figure 1, Williamson & Savage, 1986; Morley et al., 1992). Above this basement, both sedimentary and volcanic rocks are grouped into several formations (Figure 2). The oldest sedimentary rocks, the Turkana Grits Fm, consist of hundreds of metres-thick fluvial sandstones deposited between the Late Cretaceous and the

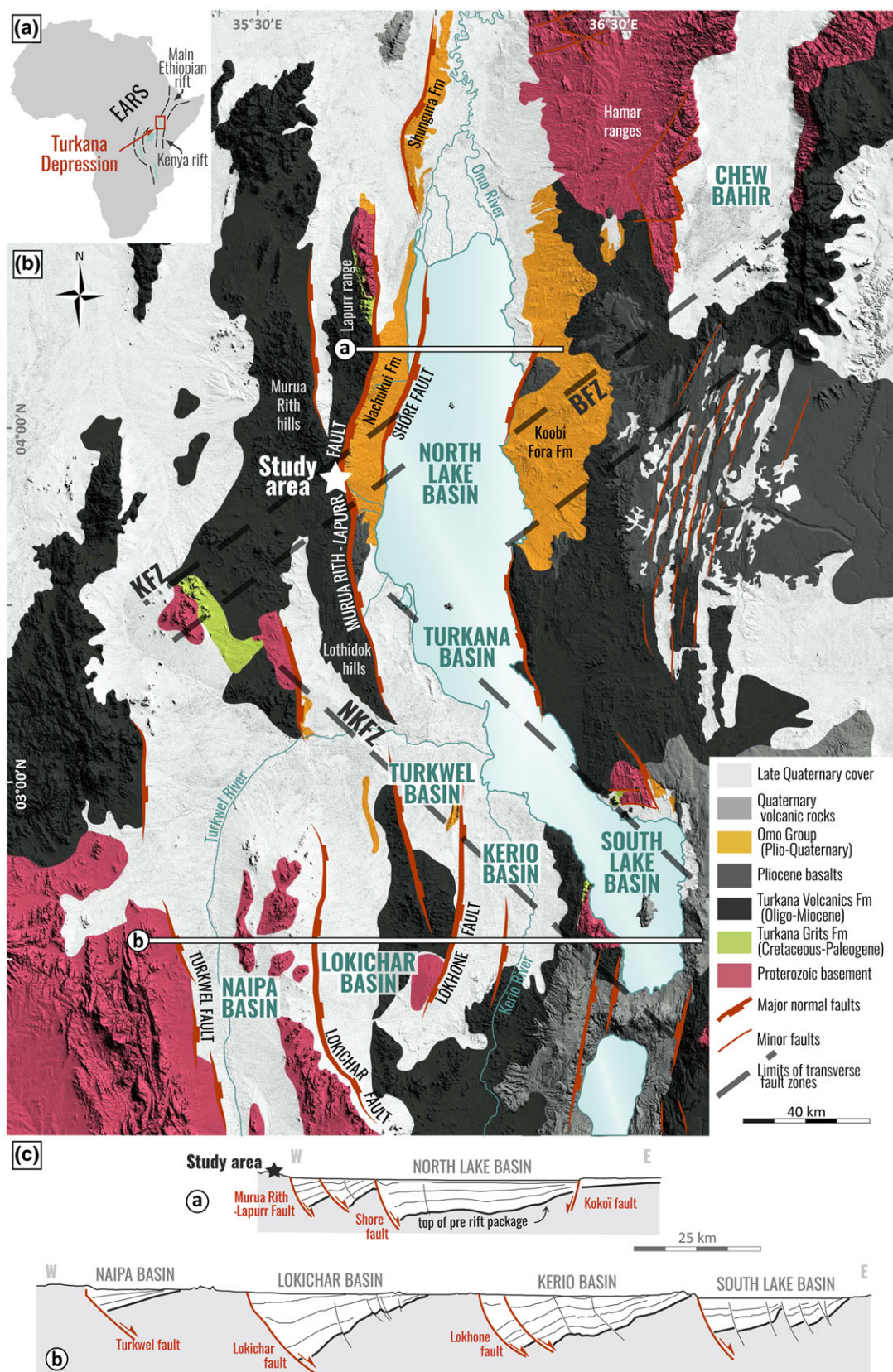


FIGURE 1 Structural and geological background of the Turkana Depression. (a) Location of the Turkana Depression, Main Ethiopian rift and Kenyan rift within the East African Rift System (EARS). (b) Geology and main structures of the Turkana Depression compiled from Walsh and Dodson (1969); Wescott, Morley, and Karanja (1993); Morley et al. (1999); Vétil (2005); McDougall and Brown (2009); and Jicha and Brown (2014). Main basins and intervening ranges are represented. Basement inherited Buluk, Kataboi, and N'Doto-Karisia fault zones (BFZ, KFZ, and NKFZ, respectively) are indicated with dashed lines. The study area is located west of the North Lake Basin and is shown with a white star. The background topography is derived from SRTM1. (c) Large-scale cross-sections showing the grabens and half-graben architectures in the northern (a) and southern (b) Turkana Depression (compiled from Wescott et al., 1999; Morley et al., 1999; Africa Oil reports, 2016) [Colour figure can be viewed at wileyonlinelibrary.com]

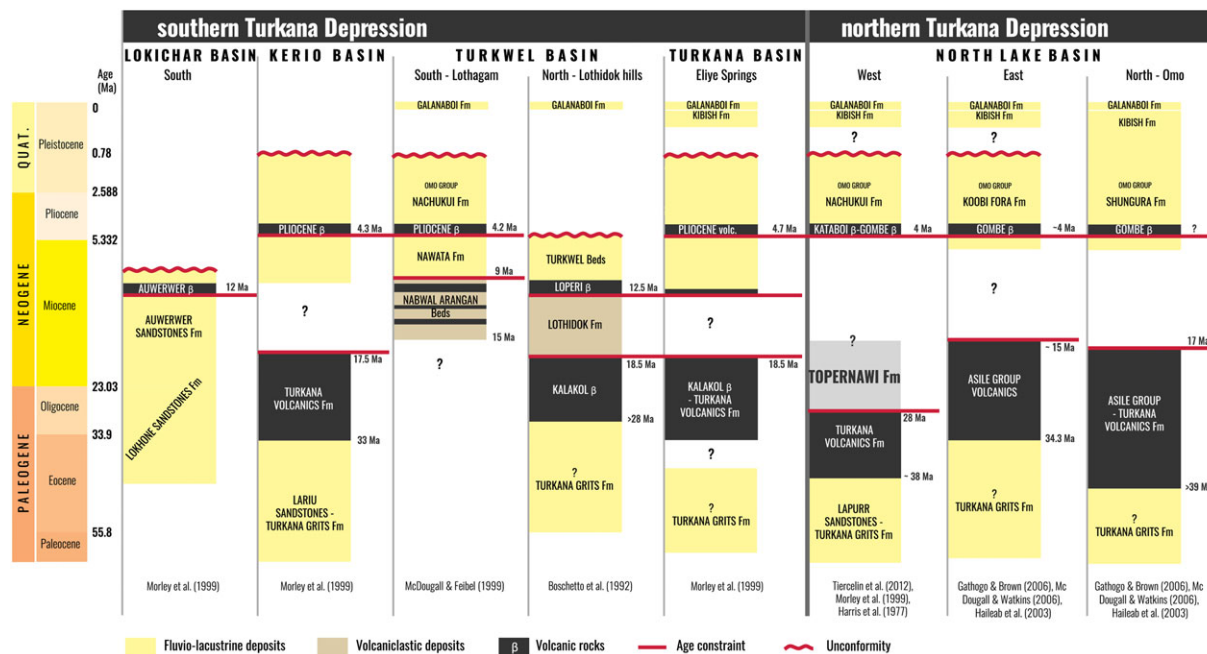


FIGURE 2 Lithostratigraphic chart of the Turkana Depression from the southernmost (left) to northernmost basins (right), based on a bibliographic synthesis (references on the figure). The age of the end of the deposition of the Topernawi Fm is discussed in the text [Colour figure can be viewed at wileyonlinelibrary.com]

Oligocene, and they are found in both the southern and northern portions of the Turkana Depression (Arambourg & Wolff, 1969; Morley et al., 1999; Muia, 2015; Thuo, 2009; Tiercelin et al., 2004; Tiercelin, Potdevin, et al., 2012; Tiercelin, Thuo, et al., 2012).

Overlying the Turkana Grits Fm, the Turkana Volcanics Formation consists of up to 3-km-thick lava flows occasionally intercalated with volcano-sedimentary rocks that are emplaced over a large portion of the Turkana Depression (Bruhn, Brown, Gathogo, & Haileab, 2011; Morley et al., 1999). The Turkana Volcanics Fm is interpreted as the result of intense fissural volcanism during the Late Eocene to mid-Miocene (Bellieni et al., 1981; Bellieni, Visentin, Piccirillo, & Zanettin, 1987; Boschetto, Brown, & McDougall, 1992; Bruhn et al., 2011; McDougall & Brown, 2009; Morley, 1994; Walsh & Dodson, 1969; Zanettin, Justin Visentin, Bellieni, Piccirillo, & Rita, 1983). This volcanism is interpreted as resulting from a coeval episode of extension (McDougall & Brown, 2009; Morley et al., 1999) that may be related to plume activity, although this remains an issue of debate (Ebinger & Sleep, 1998; Furman, Bryce, Karson, & Iotti, 2004; Furman, Kaleta, Bryce, & Hanan, 2006; Hendrie et al., 1994; McDougall & Brown, 2009; Rooney, Herzberg, & Bastow, 2012; Vétel & Le Gall, 2006). In the northern portion of the Turkana Depression (Figure 1b), the Turkana Volcanics Fm was emplaced between 39 and 28 Ma and after 20 Ma farther to the north (Figure 2, Bellieni et al., 1987; Morley et al., 1992; Morley et al., 1999; Vétel & Le Gall, 2006). To the south, the Turkana Volcanics Fm disappears progressively and is absent from the Lokichar Basin (Vétel & Le Gall, 2006).

In the Lokichar Basin, the metamorphic basement is directly overlain by the Lokhne Sandstones Fm deposited between 38 and 18 Ma (Ducrocq et al., 2010; Morley et al., 1999; Tiercelin et al., 2004). The Lokhne Sandstones Fm is syn-rift in this portion of the depression, revealing that the Lokichar Basin was already active in the Eocene (Morley et al., 1999; Vétel & Le Gall, 2006). Above the Turkana Volcanics Fm and

the coeval Lokhne Sandstones Fm, all sediments throughout the Turkana Depression are syn-rift including several formations composed of fluvio-lacustrine sediments which are, in places, intercalated by volcanic rocks (Figure 2). In the southern Turkana Depression, the syn-rift package includes the Early Miocene, mainly sandstone Auwerwer Fm (Morley et al., 1999), and its lateral equivalents the Nabwal Arangan Beds (Feibel, 2003) and the Lothidok Fm (Boschetto et al., 1992). These last two formations are overlain by the Upper Miocene to Lower Pliocene Nawata Fm (Feibel, 2003) and Turkwel Beds (Boschetto et al., 1992), respectively, which are capped by Pliocene basalts and volcanics. Formations of equivalent age are unknown or absent in the northern Turkana Depression where the Plio-Pleistocene Omo Group is the only known syn-rift deposit. The Omo Group is found throughout the entire Turkana Depression and consists of three main formations that are laterally equivalent: the Nachukui, the Koobi Fora, and the Shungura formations (Figure 2; Brown & Feibel, 1991; de Heinzelin, 1983; Gathogo & Brown, 2006; Gathogo, Brown, & McDougall, 2008; Harris et al., 1988; Nutz et al., 2017; Tiercelin et al., 2010). At the top of the Omo Group, sedimentation is more disparate and patchy. The most extensive formation is the Kibish Fm (Butzer & Thurber, 1969), also observed in southern Ethiopia, deposited between the Late Pleistocene and Early Holocene (Brown & Fuller, 2008). Finally, the most recent deposits are included in the Galana Boi Fm (Owen, Barthelme, Renaut, & Vincens, 1982), consisting of Holocene sediments unconformably overlying older sedimentary formations.

3 | METHODOLOGY

3.1 | Field geology

Following remote sensing analyses based on satellite imagery (Landsat, SRTM1, SPOT), we conducted two field surveys (October 2014 and

July 2015). We documented contacts between the Turkana Volcanics Fm and the newly recognized Topernawi Fm. The entire basin was mapped for structural and sedimentological features. We measured and analyzed four sections along incised valleys of the Topernawi River and its tributaries. We interpreted lithology, grain size, sorting, bed thickness, sedimentary structures, and paleocurrents using conventional facies analysis.

3.2 | Dating

The timing of the Ekitale Basin evolution was constrained by four samples (Table 1) dated via $^{39}\text{Ar}/^{40}\text{Ar}$ method step-heating using a CO₂ laser probe. Whole rocks were handpicked under a binocular microscope from the 0.5–1.50 mm fraction. The samples were wrapped in small Al foil package (11 × 11 mm) and stacked. Packages of fluence monitors were inserted every 10 samples. Samples were irradiated under Cd-shielding at the McMaster Nuclear Reactor (Hamilton, Canada). Sample 1 was irradiated for approximately 51 hr at a J/h of approximately $4.4 \times 10^{-5} \text{ hr}^{-1}$. The other samples were irradiated for 50 hr at a J/h of approximately $8.2 \times 10^{-5} \text{ hr}^{-1}$. Sanidine TCRs (28.608 ± 0.033 Ma; Renne, Mundil, Balco, Min, & Ludwig, 2010; Renne et al., 1998) monitored both irradiations.

We followed the $^{39}\text{Ar}/^{40}\text{Ar}$ method described in Ruffet, Féraud, and Amouric (1991) and Ruffet, Féraud, Balèvre, and Kiéna (1995). The five argon isotopes and the background baselines were measured in 11 cycles within the peak-jumping mode. Blanks were placed in each first or third/fourth run and then subtracted from the subsequent sample gas fractions. All presented isotopic measurements are corrected for K, Ca, and Cl isotopic interference, mass discrimination, and atmospheric argon contamination. Apparent age errors are plotted at the 1- σ level and do not include errors of the $^{40}\text{Ar}^*/^{39}\text{Ar}_\text{K}$ ratio, the age of the monitor nor the decay constant. The errors of the $^{40}\text{Ar}^*/^{39}\text{Ar}_\text{K}$ ratio, the age of the monitor, and the decay constant are, however, included in the final calculation of the (pseudo-)plateau age error margins or for individually cited apparent ages. A Map 215® mass spectrometer performed the analyses. It is commonly accepted that a plateau is obtained when the calculated $^{40}\text{Ar}^*/^{39}\text{Ar}_\text{K}$ ratios of at least three consecutive steps, comprising a minimum of 70% of the ^{39}Ar released, agree within the 1- or 2- σ error bars for the weighted mean of calculated $^{40}\text{Ar}^*/^{39}\text{Ar}_\text{K}$ ratios of the plateau segment. All ages are displayed at the 1- σ level. Analytical data, parameters used for calculations (isotopic ratios measured on K, Ca, and Cl pure salts, mass discrimination, atmospheric argon ratios, J parameter, and decay constants), and reference sources are available in a complementary data repository (Figure S1).

TABLE 1 Type, location, and age of dated samples

Sample	Type	Longitude (°E)	Latitude (°N)	Age (Ma)	Age error (Ma)	Reference
1	Basaltic lava flow	35.710935	3.856604	28.4	±0.1	This study
2	Dyke, oriented N30°	35.723138	3.8504722	25	±1.8	This study
3	Dyke, oriented N30°	35.726444	3.8525277	25.3	±0.1	This study
4	Dyke, oriented N05°	35.725844	3.860048	13.9	±0.1	This study
5	Basaltic lava flow	35.72	3.854	27.9	±0.3	McDougall & Brown, 2009, Sample 98–314

4 | THE EKITALE BASIN

The Ekitale Basin was initially identified from the field observation of a significant accumulation of sediments west of the Murua Rith-Lapurr Fault (MRLF, Figure 1b). Mapped sediments of the Topernawi Fm are generally bordered by faults that define a 3–5-km-wide basin directly overlying the Turkana Volcanics Fm. The Ekitale Basin is truncated to the east by the MRLF (Figure 3b) that constitutes the border fault of the North Lake Basin. The Ekitale Basin thus postdates the emplacement of the Turkana Volcanics Fm and predates the opening of the North Lake Basin. As an initial estimate, the Ekitale Basin opened and evolved between the Late Oligocene and Upper Miocene to Lower Pliocene (Figure 2). The Ekitale Basin thus belongs to the Cenozoic episode of rifting that affected the northern Turkana Depression.

Both the Ekitale Basin and the Topernawi Fm are described in detail. From field observations and stratigraphic correlations, we present a geological map showing the main sedimentary units and structural features (Figure 3a,b). A lithostratigraphic log (Figure 3c) illustrates the sedimentary succession, and four basin-scale transects expose the current architectural configuration (Figure 3d). We first describe the basement of the Ekitale Basin. Depositional environments are then reconstructed. We interpret tectonic structures and present a chronology for their emplacement. Finally, we propose a model of the tectono-sedimentary evolution of the Ekitale Basin within the framework of the Turkana Depression.

4.1 | Basement of the Ekitale Basin

The basement rocks of the Ekitale Basin (U0) consists of thick basaltic lava flows that belong to the Turkana Volcanics Fm (Figure 4a). These lava flows are characterized by metre-scale top-autobreccias covering a relatively dense core (Figure 4b,c). Some places show columnar jointing (Figure 4c). Lava flows are interpreted as aa-type to rubbly pahoehoe-type (Macdonald, 1953) and indicate subaerial spreading. We observed some intercalated pyroclastic intervals that can be affected by paleosol development, reflecting periods of volcanic quiescence. The lava flow marking the top of the Turkana Volcanics Fm in the area is dated to 28.4 ± 0.1 Ma (Sample 1, Table 1). This age is close to a previous date of 27.9 ± 0.3 Ma (Sample 5, Table 1, McDougall & Brown, 2009) attributed to the end of the deposition of the Turkana Volcanics Fm in the area.

4.2 | Sedimentary infill

The Topernawi Fm consists of a 75-m-thick sedimentary succession. It is divided into five distinct sedimentary units, named U1 through U5.

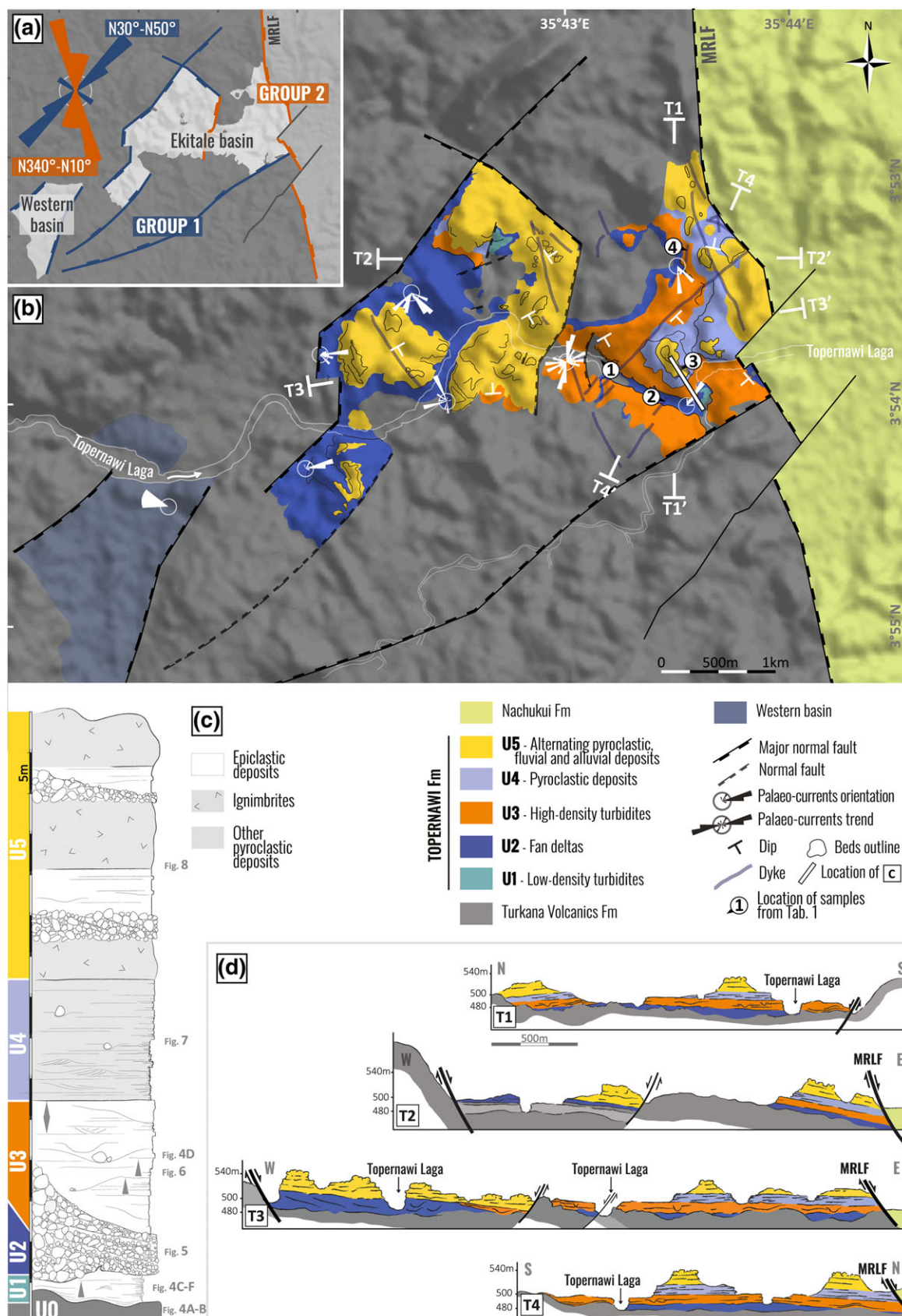


FIGURE 3 Detailed geology and structures of the Ekitale Basin. (a) Geological map of the Ekitale Basin differentiating the volcaniclastic sediments of the Topernawi Fm (light grey), basalts from the Turkana Volcanics Fm (dark grey), and clastic rocks from the Plio-Quaternary Omo Group (medium grey). Two groups of structures are delineated; Group 1 includes N30°–50° oriented faults and dykes while Group 2 consists of N340°–N10° faults and dykes. (ab) Detailed geology of the Ekitale Basin as mapped by the authors. (c) Composite stratigraphic column of the Topernawi Fm with position of relevant figures, see location Figure 3b. (d) Representative cross-sections illustrating the Ekitale Basin architecture and its relationships with the basement [Colour figure can be viewed at wileyonlinelibrary.com]

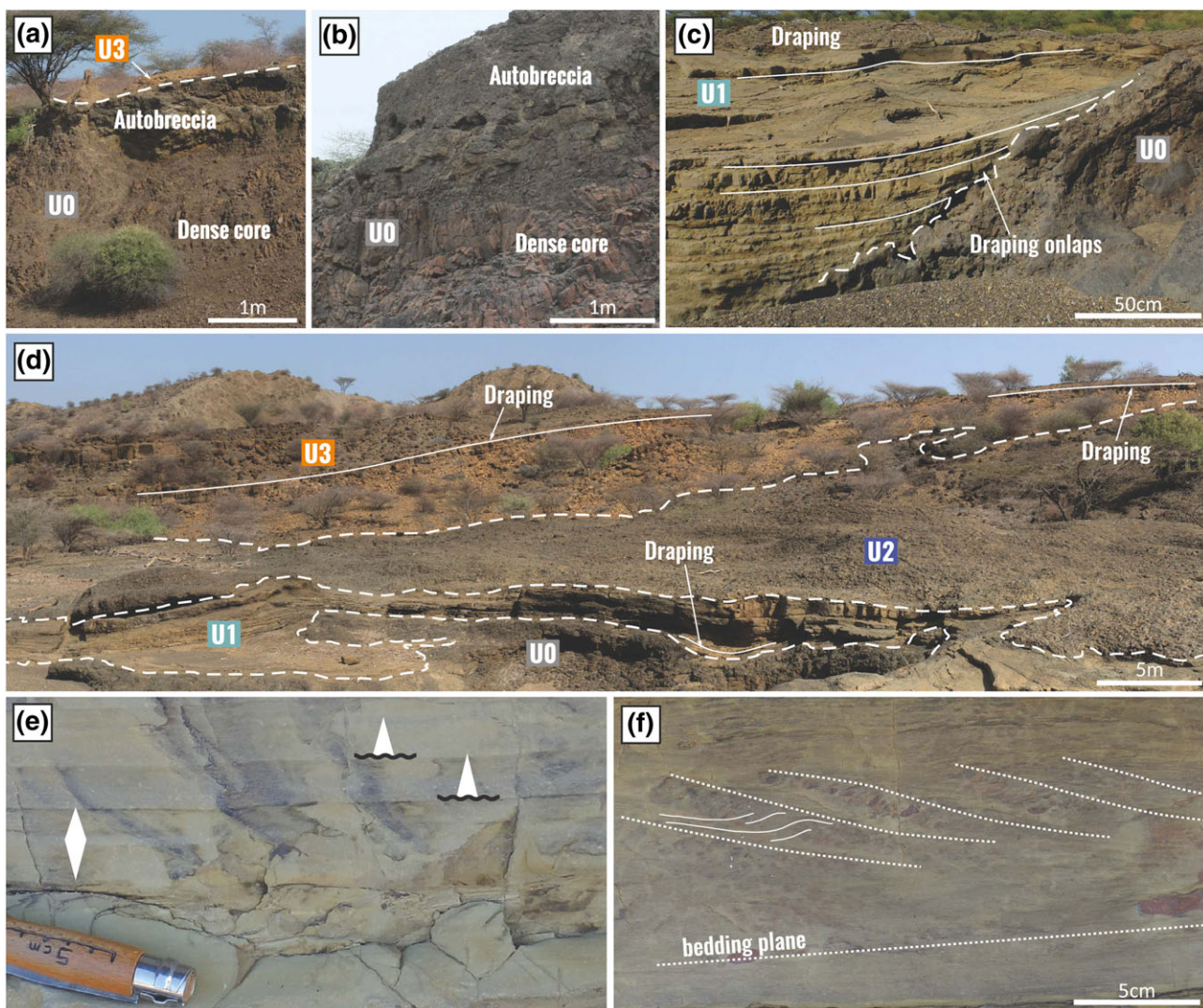


FIGURE 4 Basement of the basin and sedimentary characteristics of U1. (a) Basaltic lava flow that corresponds to the top of the basement (U0) in the central portion of the Ekitale Basin. (b) Close-up view of the dense core overlain by top-autobreccia marking the upper limit of the lava flow shown in Figure 4a. Note the columnar joints in the dense core. (c) Draping onlaps of U1 over U0. (d) Panoramic view of the central portion of the Ekitale Basin where U1, U2, and U3 crop out. Note the draping patterns of U3 over U0, U1, and U2 and the draping of U1. View toward the S-SE. (e) Centimetre-scale fining- and coarsening-up sequences in U1. (f) Stoss-depositional climbing ripples in U1, bedding plane, and stoss-sides are indicated by dotted lines while lee-sides are illustrated by continuous lines [Colour figure can be viewed at wileyonlinelibrary.com]

These sedimentary units are all volcaniclastic rocks, characterized by distinct depositional processes that allow them to be differentiated and traced throughout the basin. We follow the classification scheme of Fisher (1961) who defined three major types of volcaniclastic sediments: (a) pyroclastic deposits resulting from volcanic explosions that extrude discrete particles from volcanic vents, (b) epiclastic deposits composed of fragments produced by the erosion and the redeposition of solidified or lithified volcanic rocks, and (c) autoclastic rocks containing fragments that are produced within (but not usually extruded from) volcanic vents, during the movement of lava flows or by gas explosions within flows that have ceased to flow.

4.2.1 | U1—Complex of low-density turbidites

U1 represents a <4-m-thick package directly overlying the Turkana Volcanics Fm and is mainly observed in the central portion of the Ekitale Basin (Figure 3c). Where the slope of the underlying Turkana

Volcanics Fm is low, U1 drapes the underlaying paleotopography (Figure 4c,d). In locations where the slope is steeper, U1 intersects U0 in the form of draping onlaps (Figure 4c). U1 consists of volcaniclastic sediment in cm-scale planar laminations comprised predominantly of erosion-based, fining-up sequences with occasional coarsening-up sequences (Figure 4e) that grade from fine sand- to silt-sized grains. We also observed stoss-depositional climbing ripples (Ashley, Southard, & Boothroyd, 1982) in places (Figure 4f). Abundant mm- to cm-scale wood and coal debris is found within the sediment. Soft-sediment deformations are observed at the top of U1 marking an uneven boundary with U2 (Figure 5c).

Fining-up and coarsening-up intervals (Figure 4e) are interpreted as sediments deposited during the waning and waxing flow, respectively, of turbidity currents (Mulder & Alexander, 2001; Mulder, Migeon, Savoye, & Faugères, 2001; Mulder, Syvitski, Migeon, Faugères, & Savoye, 2003; Talling, Masson, Sumner, & Malgesini, 2012). Fine sand to silt-sized granulometry of U1 suggests low-density

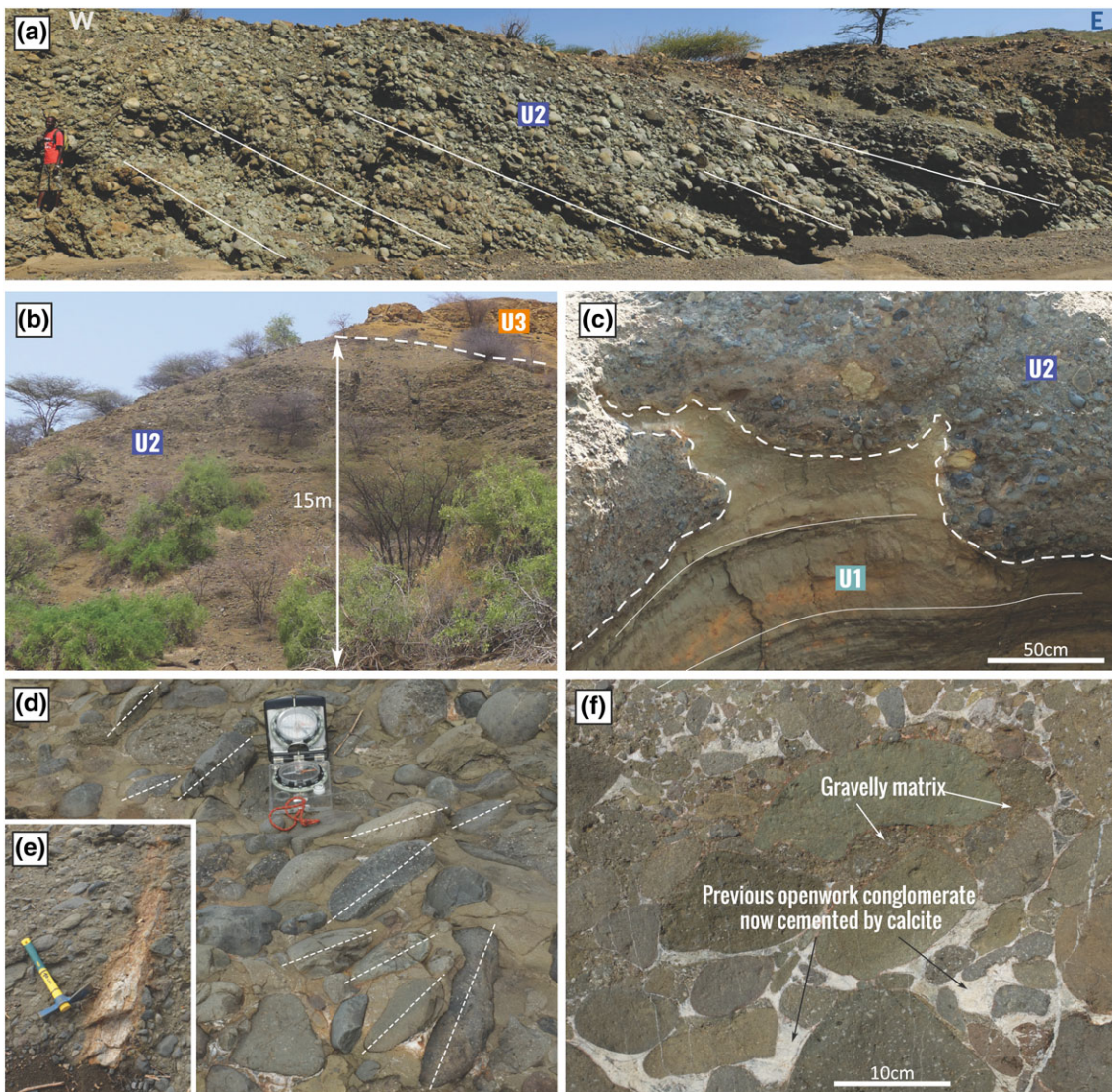


FIGURE 5 Sedimentary characteristics of U2. (a) Basinward dipping, high-angle cross-stratifications in the coarse conglomerate. (b) Coarse conglomerate of U2 conformably overlain by U3 near the northwestern faulted border of the basin. (c) Irregular contact between U1 and U2 showing recurrent post-depositional intrusions of U1 into U2. (d) Oriented and imbricated basaltic clasts. (e) Wood trunk remnant. (f) Coarse conglomerate showing partial precipitated calcite cement testifying to previous openwork [Colour figure can be viewed at wileyonlinelibrary.com]

turbidity currents (Talling, Masson, Sumner, & Malgesini, 2012). Fine sand to silt-sized granulometry of U1 suggests low-density turbidity currents (Talling et al., 2012). Stoss-depositional climbing ripples (Figure 4f) reflect unidirectional flow associated with high suspended loads, a feature also compatible with low-density turbidity currents (Jobe, Lowe, & Morris, 2012; Talling et al., 2012). The general draping pattern of U1 (Figure 4d) suggests either a subaqueous deposition or deposition from hot pyroclastic flows. The lack of fiammes, ballistic clasts, or accretionary lapilli, normally associated with hot genetic flows, supports the interpretation of water-related turbidity currents. Furthermore, soft-sediment deformations along the top boundary of U1 occur in water-saturated sediments (Owen, 1996; Owen & Moretti, 2011) and confirm a subaqueous depositional environment. Thus, we conclude that U1 is composed of epiclastic rock (Fisher, 1961; Pettijohn, Potter, & Siever, 2012) deposited by low-density turbidity currents and hyperconcentrations originating from the distal sedimentation of a turbiditic complex related to a sediment-laden river flowing (Mulder et al., 2003; Zavala, Arcuri, Meglio, Diaz, & Contreras,

2011) into a lake. Moreover, the presence of abundant wood debris suggests that water drained a vegetated subaerial area, again supporting this interpretation (Zavala, Arcuri, & Valiente, 2012).

4.2.2 | U2—Alluvial fan deltas

U2 is a clast-supported conglomerate (Figure 5) that comprises wedge forms of up to 15 m in thickness and fringing the northwestern border faults. This unit thins laterally to 1–2 m thick toward the central portion of the basin (Figure 5a). Clasts consist of 2 to 30 cm well-rounded and relatively well-sorted basalts and phonolites (Figure 5d,f), while the matrix consists of gravelly to coarse sand-sized material (Figure 5f). The lower boundary of this unit is irregular due to recurrent intrusions of U1 into U2 (Figure 5c). U2 often displays relatively high-angle oblique stratifications (15° – 35°) that dip basinward (Figure 5a). Imbricated clasts indicate a paleoflow direction toward the central portion of the basin (Figure 5d). In places, an openwork conglomerate is observed (Figure 5f) as well as 2–10-m-wide channel forms that

occasionally scour the oblique stratifications. Finally, 1–40 cm silicified wood debris are common, including fossil wood trunks up to 2 m long (Figure 5e).

In the wedge forms, basinward oblique stratifications are interpreted as foreset beds prograding from the basin margins toward the central portion (Figure 5b). Very large clasts (Figure 5d,e) might suggest a transport by relatively high-energy flows over a rather short distance. The maximum thickness of clinoforms close to border faults testify to a genetic linkage to these border faults. We interpret this unit as epiclastic rocks deposited in alluvial fans that partly fringed the basin. The intrusions of U1 into the overlying U2 relate to the presence of water-saturated sediments that reflect a subaqueous environment where U2 is deposited onto U1 (Figure 5c). Openwork conglomerates (Figure 5f) also support our interpretation of a subaqueous environment where the winnowing of the conglomerate matrix can be related to subaqueous currents or waves in the nearshore to shoreface domains (Hart & Plint, 1995). The subaqueous emplacement of the foreset beds indicates that these alluvial fan deltas deposited along the shore of a lake. Occasional high-angle foreset bedding suggests that these alluvial fan deltas developed into, at least episodically, Gilbert-type fan deltas (Postma, 1990), reflecting periods of higher lake stands. These alluvial fan deltas correspond to syn-tectonic deposits having been fed by the dismantling of the topography created by border fault activity or by more distal sources in the Turkana Volcanics Fm.

4.2.3 | U3—Complex of high-density turbidites

U3 consists of a 20-m-thick tabular interval draping the underlying U0, U1, and U2 units (Figure 4d). U3 consists of volcaniclastic sand- to gravel-sized sediments. Meter-scale tabular beds are dominant although they are frequently reworked by <10-m-wide and 1–4-m-thick channel forms (Figure 6a–c). Planar beds include erosive-based, fining-up sequences that occasionally contain coarsening-up, dm-scale sequences composed of gravel- to sand-sized grains (Figure 6d). Parting lineations are frequently observed in the sand-sized material (Figure 6e). In places, planar beds are composed of cm-scale pebbles (Figure 6c). Channel forms are generally filled by slightly coarser material than the surrounding planar beds (Figure 6f). They consist of massive to faintly laminated beds of coarse sand-sized grains to pebbles in dm-scale fining-up sequences. These sequences occasionally contain cross-stratifications and current ripples. In places, channel forms comprise outsized clasts of more than >20 cm that mantle the basal erosion surface (Figure 6c). In places, gutter casts are found at the base of some channel forms. Finally, silicified cm- to m-scale wood debris, trunks, and coal clasts are often found in both the channels and planar stratifications.

The fining- and coarsening-up sequences (Figure 6d), found in both the planar beds and channel forms, are interpreted as the waxing and waning flows, respectively, of turbidity current deposits (Mulder et al., 2001; Mulder et al., 2003; Mulder & Alexander, 2001; Talling et al., 2012). As with U1, the general draping pattern of U3 over the underlying units (Figure 4d) suggests either a subaqueous deposition or a deposition from hot pyroclastic flows. Again, the absence of any indicators for hot flows supports subaqueous turbidity currents as

the origin of U3. In places, a waxing sequence directly overlies a waning sequence (Figure 6d). The preservation of deposits related to the waxing flow (Figure 6d) is traditionally associated with hyperpycnites. This interpretation is also supported by the abundant wood remains, testifying to the drainage of subaerial areas by rivers and deposition into a lake. Massive to faintly laminated material, including the outsized clasts in the channel forms, are attributed to debris flow to high-density turbidity currents (Kneller, 2003; Mutti, Tinterri, Benevelli, di Biase, & Cavanna, 2003; Talling et al., 2012). Thus, U3 consists of epiclastic sediments deposited in the form of both high-density turbidites and debrites (Talling et al., 2012) related to debris flows and high-density flows due to a river entering a lake. The lack of progressive transition between alternating planar and channelized beds suggests that they are related to variable energetic conditions associated with the successive turbidity currents, rather than to progradation or retrogradation. The channel forms (Figure 6a–c,f) reflect laterally confined turbidity currents and a relatively greater energetic flow from more powerful flood events (Wright, 1977). Planar beds develop from flows in the more distal domain or during less energetic flows. We interpret U3 as a complex of proximal to intermediate turbidites in a sub-lacustrine environment.

4.2.4 | U4—Pyroclastic deposits

U4 consists of a >20-m-thick succession conformably overlying U3 (Figure 7a). It is composed of volcaniclastic sediments, comprising reddish medium sand-sized grains alternating with whitish gravelly-sized to coarse sand-sized grains forming dm-scale beds (Figure 7a,b). In the lower portion of the unit, beds are 0.1–0.3-m-thick and usually include alternating planar and low-angle oblique tangential laminations which are generally westward dipping at 10°–15° (Figure 7b). The low-angle laminations are truncated and are overlain by relatively continuous layers that drape the upper undulating surface, slightly thickening above the truncated laminations (Figure 7b). In the upper portion, planar laminations dominate. Centimetre- to dm-scale clasts are common in the sandy sediments. Laminations show asymmetric plastic deformation below these floating outsized clasts (Figure 7c). In places, U4 includes cm-scale beds of 1–3 mm diameter spherical clasts that have concentric laminations (Figure 7d,e).

We interpret the floating clasts as ballistic clasts (Cas & Wright, 1988) and the spherical clasts within the cm-scale beds as accretionary lapilli (Gilbert & Lane, 1994). Thus, we consider U4 as a pyroclastic deposit. Alternations of planar and low-angle oblique laminations (Figure 7b) reflect the alternating development of upper stage plane beds and dunes and relate to alternating sub- and supercritical flows (Alexander, Bridge, Cheel, & Leclair, 2001; Duller, Mountney, Russell, & Cassidy, 2008; Fielding, 2006; Schmincke, Fisher, & Waters, 1973). This dune bedding has numerous similarities with the progressive “type A” dunes of Cole (1991), interpreted as pyroclastic-surge deposits. The orientation of the dunes and the direction of the asymmetric deformations below the ballistic clasts also support a pyroclastic flow originating from the east. We interpret U4 to be a base surge deposit (Moorhouse & White, 2016; Walker, 1984; Waters & Fisher, 1971; Wohletz & Sheridan, 1979) attributed to pyroclastic flows (Fisher & Schmincke, 1984; Waters & Fisher, 1971).

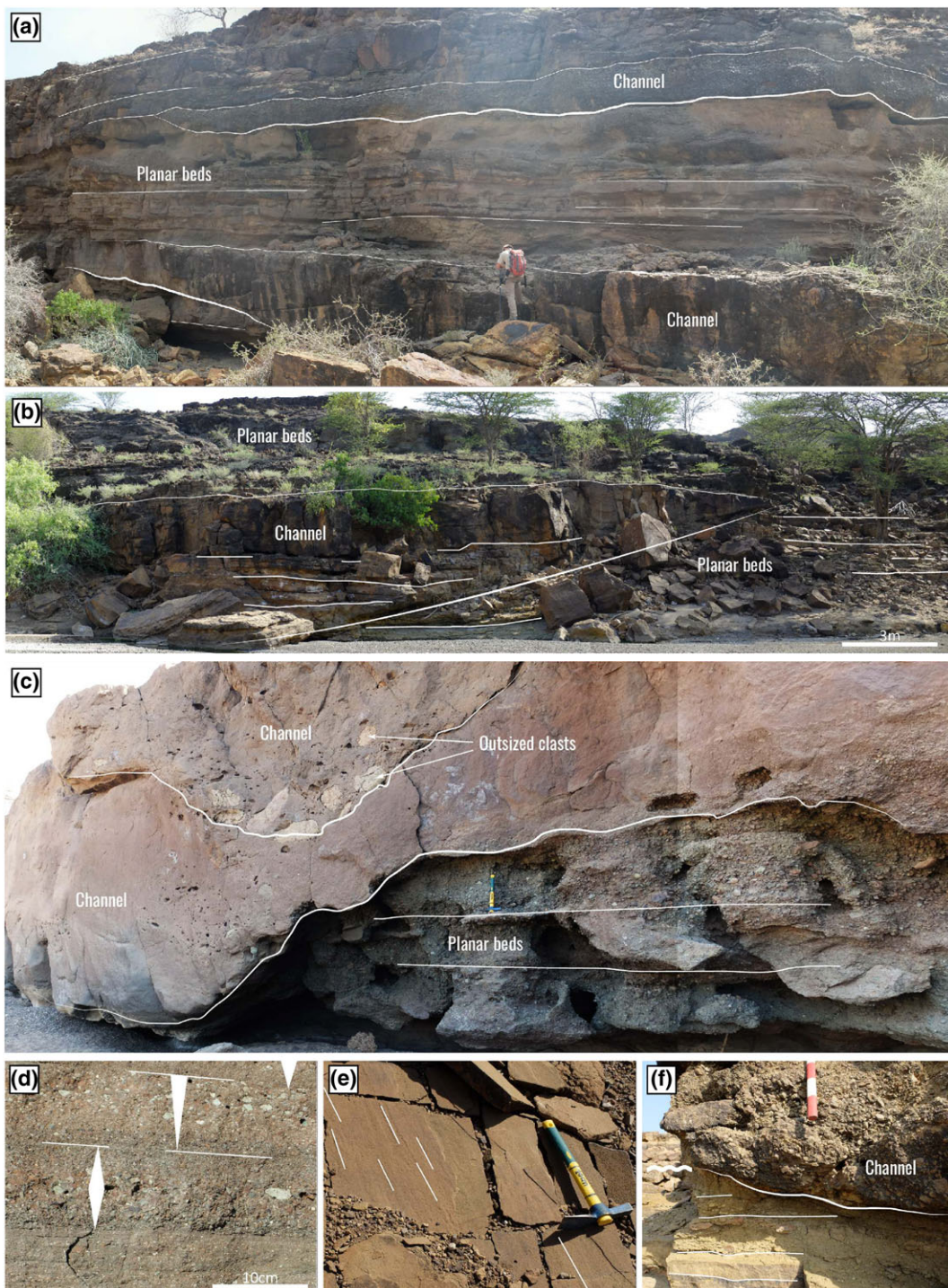


FIGURE 6 Sedimentary characteristics of U3. (a-c) Alternations of planar and channelized intervals. Channels are faintly laminated to massive and occasionally outsized boulders underline the erosional trough. (d) Decimetre-scale fining- and coarsening-up sequences in planar beds. (e) Parting lineations in planar beds. (f) Channelized medium conglomerate that eroded the underlying planar beds [Colour figure can be viewed at wileyonlinelibrary.com]

4.2.5 | U5—Alternating pyroclastic, fluvial, and alluvial deposits

U5 is a 30–50-m-thick sedimentary unit. Conformably overlying U4, U5 can be traced throughout the basin by its yellow to purple color stemming from an intense weathering that is often characterized by spheroidal weathering (Figure 8b) in the uppermost part of the succession. U5 is composed of volcaniclastic sediments. In places, the

primary sedimentary structures are difficult to observe; however, we can divide U5 into three main facies associations. The first facies association consists of sand-sized grains including mm- to cm-scale floating angular clasts and frequent fiammes in structureless to faintly stratified 5–20-m-thick tabular intervals (Figure 8a,c,d,e). The second facies association is comprised of horizontally stratified gravels in 2–10 m tabular intervals (Figure 8a,c,f). The tabular intervals are recurrently incised by channel forms filled mostly by clast-supported

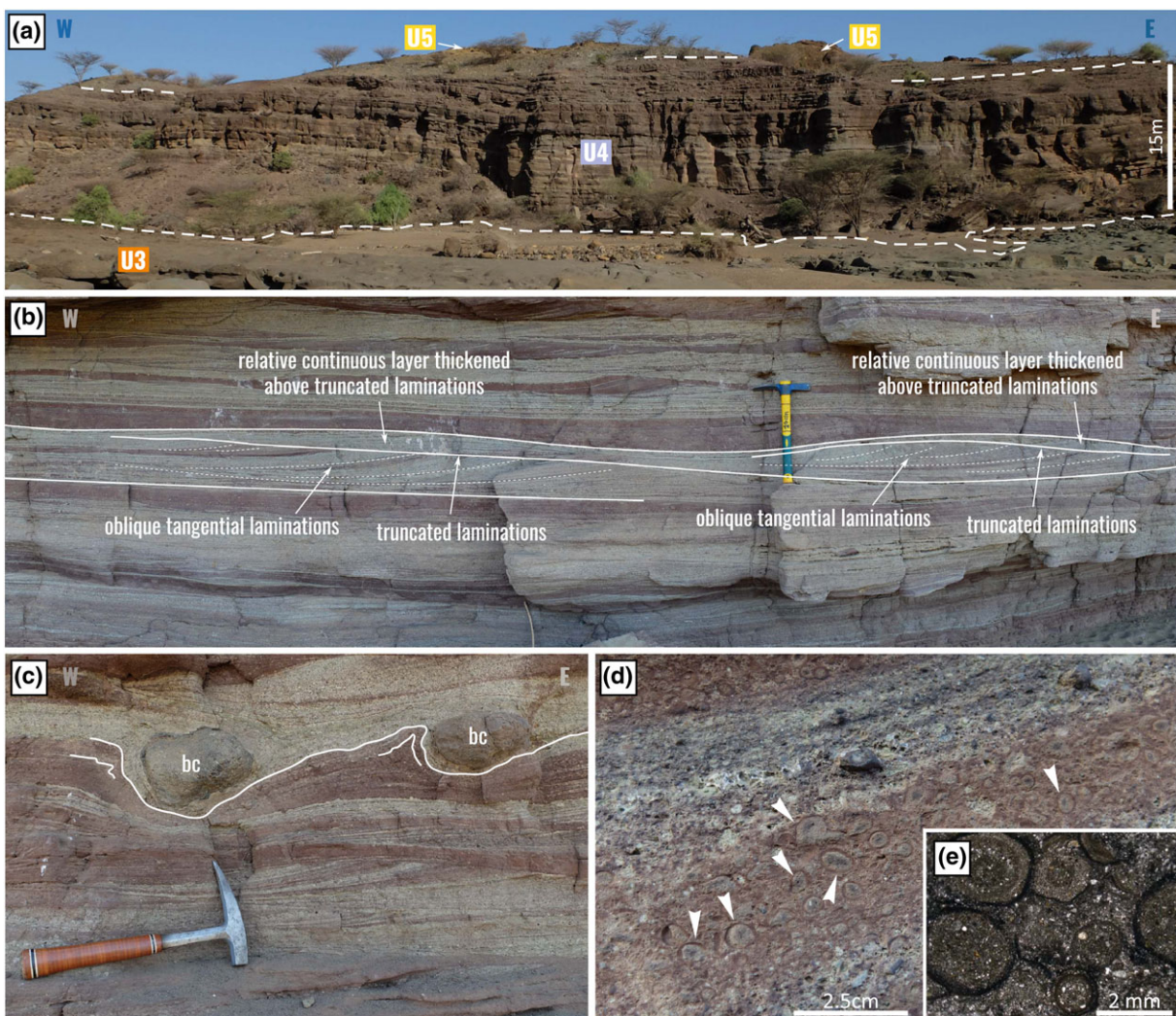


FIGURE 7 Sedimentary characteristics of U4. (a) U4 conformably overlies U3 and is overlain by U5 in the central portion of the basin. (b) Detail of dunes in the lower part of U4. They are characterized by dm-scale tangential cross-laminations. (c) Decimetre-scale ballistic clasts (bc). (d) Example of a cm-scale bed composed of spherical clasts (white arrow heads). (e) Thin sections of spherical clasts characterized by concentric micro-laminations interpreted as accretionary lapilli [Colour figure can be viewed at wileyonlinelibrary.com]

conglomerate composed of well-sorted cm-scale rounded to well-rounded pebbles (Figure 8f). The third facies association is a matrix-supported coarse conglomerate (Figure 8c,g) included within >10-m-thick wedge forms. These wedge forms are particularly well developed near the border faults of the basin (Figure 8g) and pinch out toward the central portion. Large-scale oblique stratifications are observed on occasion (Figure 8g). These conglomeratic intervals contain abundant silicified wood remains and coal debris.

The structureless and faintly stratified pattern coupled with the absence of a muddy matrix suggest that the first facies association was formed by deposits from high-density turbidity currents (Mulder & Alexander, 2001). However, fiammes (Figure 8d,e) testify to hot genetic flows; thus, the first facies association are interpreted as ignimbrites (Smith, 1960; Wilson & Walker, 1982) deposited by pyroclastic flows. The sorting of clasts within the channel forms of the second facies association and the absence of finig- and coarsening-up intervals suggest a relatively long-term transport by dilute flow rather than transport by successive turbidity currents. We interpret channel forms as evidence of fluvially remobilized pyroclastic material. The

horizontally stratified tabular beds are inferred as overbank deposits associated with fluvial floods. Finally, coarse conglomerate within the third facies association (Figure 8c,g) suggests high-energy and short-distance transport (ten to few tens of kilometres). The maximum thickness of this facies along the basin margins suggests a genetic connection with border faults. We interpret the wedge-shaped, large-scale oblique stratifications as foresets similar to those in U2. The clinoforms are interpreted as alluvial fan progradation genetically related to border fault activity. In summary, U5 includes alternating deposits derived from pyroclastic events, fluvial drainage in the central portion of the basin during volcanic quiescence (Figure 8c), and alluvial fan development during border fault activity. Weathering of U5 (intense and spheroidal) testifies to a long-term exposure of the uppermost surface after its deposition, rather than a recent denudation.

4.2.6 | Synthesis

The stratigraphic units indicate that two main phases of sedimentation occurred in the Ekitale Basin. The first phase is characterized by the appearance and evolution of a lacustrine system which directly overlies

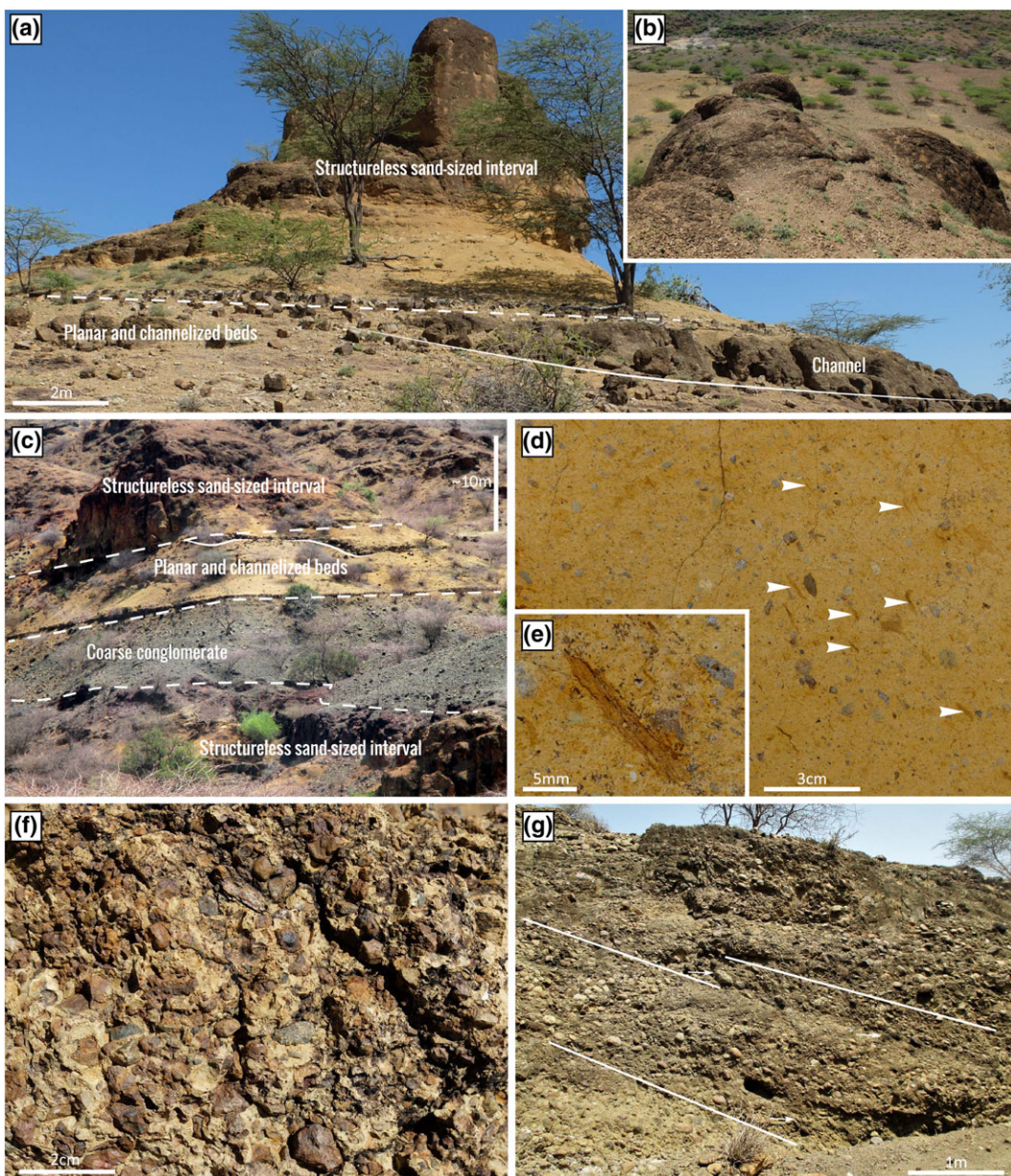


FIGURE 8 Sedimentary characteristics of U5. (a) Yellow to purple sediments corresponding to the uppermost part of U5 in the central portion of the basin. This includes gravel- to pebble-sized material in planar and channelized beds (second facies association) conformably overlain by structureless sand-sized material (first facies association). View toward the North of the Ekitale Basin. (b) Spheroidal weathering at the top of U5 affecting the structureless sand-sized material. (c) Yellow to purple sediments of U5 displaying alternations of intervals made of structureless sand-sized material (first facies association), gravel- to pebble-sized planar and channelized beds (second facies association), and coarse conglomerate (third facies association). (d) Details of structureless sand-sized material composed of mm- to cm-scale floating sub-angular to angular clasts and fiammes (white arrows) in sand-sized material. (e) Close-up view of a fiamme. (f) Mostly clast-supported fine conglomerate in a channelized form (second facies association). (g) Thick and coarse conglomerate located near the border fault of the basin showing internal large-scale oblique stratifications. Imbricated clasts are highlighted with white arrows [Colour figure can be viewed at wileyonlinelibrary.com]

the Turkana Volcanics Fm. This lake was fed by alluvial and fluvial systems (U1, U2, and U3) and thereby shows that the Ekitale Basin hosted a small river-driven lake (*sensu* Nutz, Schuster, Ghienne, Roquin, & Bouchette, 2018). During this period, border fault activity was relatively important, and the Ekitale Basin was underfilled, allowing the development of a perennial lake. During the second phase, the prevalence of pyroclastic deposits indicates a renewal of local volcanism. Pulses of fault activity, expressed by the development of alluvial fans in U5, continued to create accommodation space. However, this second phase is characterized by excessive sediment supply and the Ekitale Basin

became overfilled. This led to the disappearance of the former lake and to a sedimentation dominated by volcanic events and fluvial/alluvial deposits. Finally, there was a long-lasting non-depositional period inferred from the intense weathering at the top of U5, suggesting that sedimentation was interrupted after the deposition of U5. The Topernawi Fm is believed to have recorded the complete history of the basin.

4.3 | Structural characterization

Numerous faults and volcanic dykes were identified in the Ekitale Basin through remote sensing and field mapping. According to their

relationships with sediments of the Topernawi Fm and their orientation, we divided these faults and dykes into two main structural groups.

4.3.1 | Group 1

This group includes N30°–50°-oriented normal faults that systematically separate rocks of the Turkana Volcanics Fm—forming footwalls—from rocks of the Topernawi Fm, which correspond to hanging walls (Figure 3b). To the north, 3.5-km- and 6-km-long SE-dipping normal faults oriented N40° mark the limit of the Ekitale Basin (Figure 3b). To the south, the Ekitale Basin is bordered by a 6-km-long NW-dipping normal fault oriented N50° (Figure 3b). Along both the northern and the southern limits, the faults are marked by escarpments of ten to several tens of metres in height (Figure 9a). A 3-km-long segment of the northern limit consists of a N140° normal fault. This fault separates the Turkana Volcanics Fm from the Topernawi Fm, and we thus included this in Group 1. Finally, two N30°–40° trending normal faults, 2 and 4 km long, delineate the western basin (Figure 3a) and are thus included in Group 1.

Structures belonging to Group 1 limit both the Ekitale and western basins, and they never truncate their sedimentary infills. Moreover, the genetic relationship between the normal faults of Group 1 and the development of associated alluvial fans (units U2 and U5) testifies to a recurring pulsed activity of Group 1 normal faults during the deposition of the Topernawi Fm. Thus, Group 1 normal faults are syn-sedimentary structures. Group 1 structures created the accommodation space necessary for the deposition of the Topernawi Fm. The dominant orientation of the Group 1 structures (N30°–50°) is similar to the orientation of structures belonging to the basement-inherited

fault zones KFZ and BFZ (Vétel, 2005; Vétel & Le Gall, 2006). We thus interpret the development of Group 1 structures to be associated with the extensional reactivation of pre-existing structures. The N140° segment, incorporated in Group 1, is attributed to the reactivation of conjugate structures. Structures of similar orientation are identified both in the KFZ and BFZ (Vétel, 2005; Vétel & Le Gall, 2006).

4.3.2 | Group 2

The second group includes both normal faults and volcanic dykes. They differ from Group 1 structures as they systematically cross-cut the Topernawi Fm. Most of the structures are oriented between N340° and N10° highlighting a general N-S orientation. Two main normal faults are included in this group (Figure 3a). The first corresponds to the MRLF fault that borders the Ekitale Basin to the east. In the study area, the MRLF is oriented N350° and truncates the Topernawi Fm (Figure 3a,b), separating the current rift shoulder from the North Lake Basin (Figure 1b). The second is located 2 km westward and consists of a 2-km-long N10° west-dipping normal fault (Figure 3b). This fault cross-cuts the entire Topernawi Fm with a vertical offset of about 10 m (Figure 9b,d). In addition, most of the basaltic dykes (Figure 9c) that truncate the entire Topernawi Fm are oriented between N340° and N10° and are thus included in Group 2. One of these dykes has been dated at ca. 14 Ma (Sample 4, Table 1). N30°–40°-oriented dykes that share orientations with Group 1 structures—rather than the usual Group 2 orientations—have also been identified. Two of them have been dated ca. 25 Ma (Samples 2 and 3, Table 1).

All normal faults and dykes belonging to the Group 2 cross-cut the Topernawi Fm and thus postdate the deposition of the Topernawi Fm.

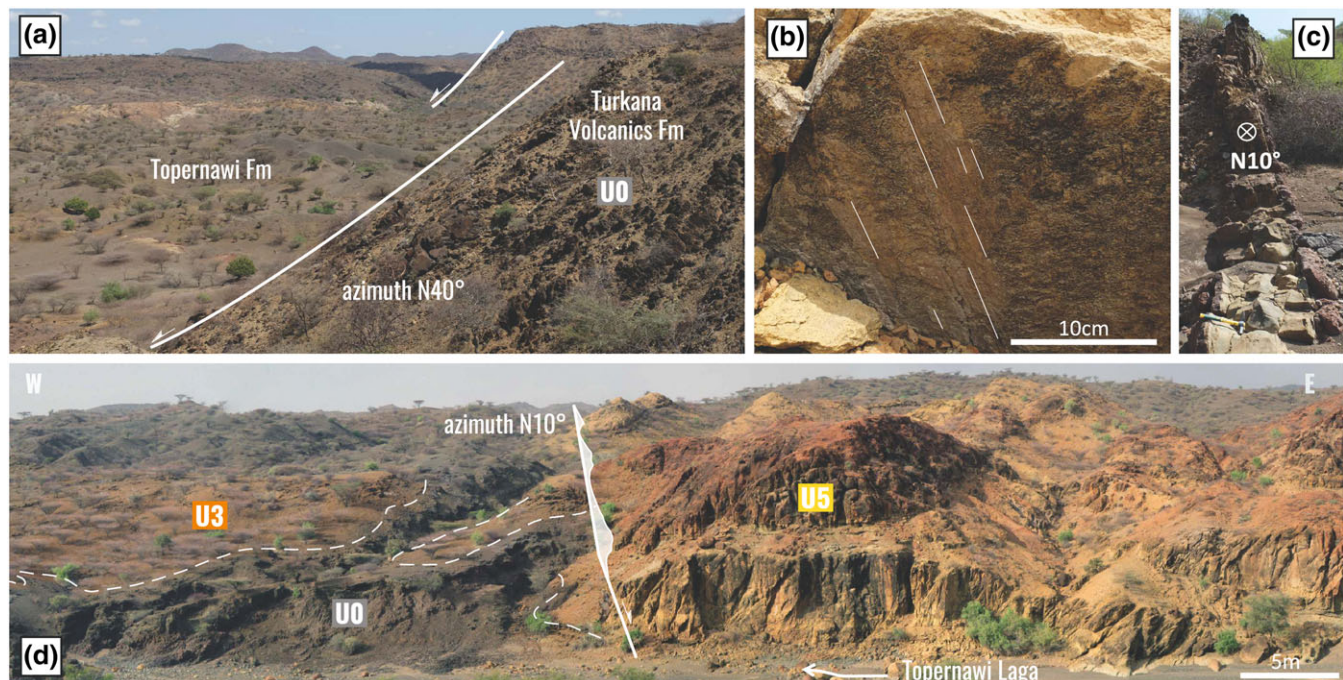


FIGURE 9 Examples of structural characteristics of the Ekitale Basin. (a) Group 1 normal fault at the northern limit of the basin. The escarpment is 50 m high and separates the Turkana Volcanics Fm (U0) from the Topernawi Fm. (b) Striations on the plane of the fault shown in Figure 9d (Group 2) highlighting a dip-slip movement. (c) Example of basaltic dyke cross-cutting the Topernawi Fm. The dyke is oriented N10° and is included in the Group 2 structures. (d) Example of a Group 2 normal fault cross-cutting the Topernawi Fm in the central portion of the basin [Colour figure can be viewed at wileyonlinelibrary.com]

Therefore, Group 2 normal faults reflect a more recent extensional episode. This second extensional event led to previously active faults being abandoned and the generation of new, broadly N-S-oriented structures in the Ekitale Basin. One of these Group 2 structures is the MRLF that started to develop with the opening of the North Lake Basin (Vétel & Le Gall, 2006). Thus, N-S-oriented structures included in Group 2 are interpreted as being coeval with the opening of the North Lake Basin and more generally with the pervasive development of N-S-oriented basins in the Turkana Depression. Having a similar range of orientations, N-S-oriented dykes are interpreted to have developed broadly coeval to the Group 2 normal faults and thus to the opening of the North Lake Basin. Furthermore, N30°–40°-oriented dykes are oriented in a similar manner as the Group 1 structures, suggesting they are associated to another event. This is supported by absolute ages (Table 1) confirming that the N30°–40° and N-S-oriented dykes were emplaced during two separate events dated at *ca.* 25 and *ca.* 14 Ma, respectively.

4.4 | Chronological constraints

Based on the available dating (Table 1), several key periods in the history of the Ekitale Basin can be defined. Sedimentation in the Ekitale Basin began after *ca.* 28 Ma (age of the last lava flows [U0] that predate deposition of the Topernawi Fm). The duration between the deposition of the last lava flows and the first lacustrine (U1) and alluvial fan delta deposits (U2) remains unknown. Yet, at the top of the last lava flows, there is an absence of a pervasive and well-developed paleosol as well as a lack of thin fluvial- or run-off-derived sediment cover. This makes unlikely the possibility of a long exposure prior to the deposition of U1 and suggests a relatively rapid initiation of deposition in the Ekitale Basin following the emplacement of the Turkana Volcanics Fm. Additionally, the oldest dykes that cross-cut the Topernawi Fm are dated *ca.* 25 Ma. Therefore, the Topernawi Fm was deposited between *ca.* 28 and *ca.* 25 Ma, indicating the Ekitale Basin evolved during this time interval. The next important event affecting the Ekitale Basin was the activation of the N-S structures (Group 2 faults and dykes) and the opening of the North Lake Basin. The timing of the MRLF activation has been recently estimated between 15 and 9 Ma based on thermochronology (Boone et al., 2018). This is supported by the age of a N-S-oriented Group 2 dyke dated *ca.* 14 Ma (Table 1), interpreted as coeval to the development of N-S normal faults. We thus consider the Ekitale Basin to have opened *ca.* 28 Ma and the sedimentation to have been interrupted *ca.* 25 Ma. We also confirm that the North Lake Basin opened *ca.* 14 Ma leading to the definitive inversion of the Ekitale Basin, likely because of the uplift of the rift shoulder.

4.5 | Tectono-sedimentary evolution of the Ekitale Basin

Combining sedimentary and structural analyses, we can summarize the evolution of the Ekitale Basin from its initiation through to its inversion. Major tectonic events and sedimentary dynamics that impacted

the Ekitale Basin are integrated into a model of the basin's evolution (Figure 10).

After the deposition of the Turkana Volcanics Fm *ca.* 28 Ma (Figure 10a), the Ekitale Basin opened due to a first extension phase that reactivated pre-existing N30–50°-oriented basement-inherited structures. This led to the development of a depocenter at the top of the Turkana Volcanics Fm (Figure 10b) and allowed the onset of deposition of the Topernawi Fm. Rapidly, this newly formed depression collected water from several rivers that drained the Turkana Volcanics Fm to form a lake. In the same time, alluvial fan deltas (U2) developed along the active border faults, fed directly by sediments originating from the dismantling of the newly created footwalls (Figure 10b). At the distal portion of alluvial fan deltas, rivers periodically generated hyperpycnal flows during flood episodes to produce low-density turbidites (U1, Figure 10B). Progressively, the activity of border faults reached a climax, and the topography reached a maximum (Figure 10c,d). This increased the production of coarse material from the erosion of the footwall to, in turn, supply alluvial fan deltas (U2). The deltas prograded toward the central portion of the basin (Figure 10c). At the same time, a river system was captured and progressively fed an important turbiditic complex (U3, Figure 10d). Given the amount and the nature of sediment, this river system appears to have represented the axial system of the basin as opposed to the transverse system represented by smaller rivers that fed the alluvial fan. Subsequently, one or several volcanic centres located east of the Ekitale Basin generated a first important pyroclastic pulse (U4, Figure 10e). Other pyroclastic events followed and –during periods of inactive volcanism—rivers drained the basin (Figure 10f). The Ekitale Basin evolved as such until its interruption likely at the end of activity along the border faults with the ceasing of extension, slightly before 25 Ma (Figure 10g). Weathering then progressively affected the area of the Topernawi Fm characterized by tectonic quiescence and non-deposition during an almost 11 Ma long period (Figure 10g, h). Around 14 Ma, N-S faulting was initiated and segmented the Ekitale Basin (Figure 10h). From then, the general uplift of the area due to its new position in the rift shoulder of the North Lake Basin led to the inversion of the Ekitale Basin. Currently, the Ekitale Basin overlies the Turkana Volcanics Fm on top of the footwall of the North Lake Basin. East of the MRLF, a portion of the Ekitale Basin is likely buried under several kilometers of syn-rift sediments deposited in the North Lake Basin.

5 | IMPLICATIONS FOR EVOLUTION OF THE EARS IN THE TURKANA DEPRESSION

Together with the Afar region (Bosworth, Huchon, & McClay, 2005; Macgregor, 2015), the Turkana Depression is an area of the EARS that has been active since the onset of Cenozoic rifting, from *ca.* 35 Ma to the present (Macgregor, 2015). The newly described fill of the Ekitale Basin provides convincing evidence for an earlier phase of rifting than previously recognized in the northern Turkana Depression which now needs to be incorporated into the Cenozoic rifting history of the region. Here, we discuss the timing of the opening of both the Ekitale and the North Lake basins in relation to the

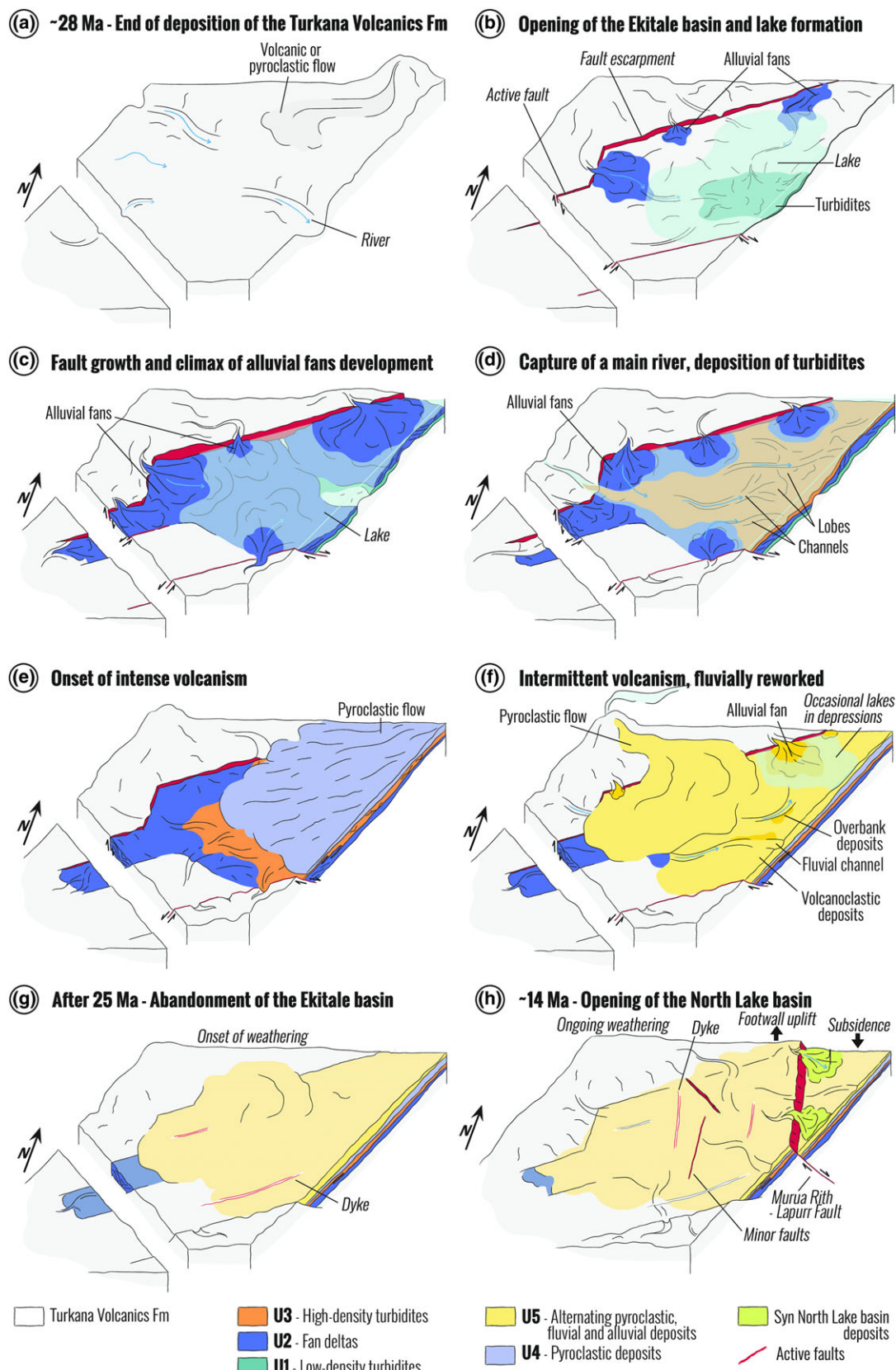


FIGURE 10 Scenario for the tectono-sedimentary evolution of the Ekitale Basin. (a) Deposition of the Turkana Volcanics Fm ends ca. 28 Ma. From (b) to (d), the Ekitale Basin opens, and the first phase of sedimentation is characterized by the evolution of a river-driven lake. Sedimentation is controlled by alluvial fans from the border faults and rivers that fringe the lake. In (e) and (f), the second phase of sedimentation is characterized by renewed volcanic activity. Sedimentation is controlled by volcanic centres that triggered repeated pyroclastic deposits, interbedded by fluvial and alluvial sedimentation during volcanic quiescence. (g) After 25 Ma, border faults no longer accommodate the extension, leading to the abandonment of the basin. A period of tectonic quiescence begins, lasting ca. 10 Ma. (h) At ca. 14 Ma, the North Lake Basin opens and the MRLF truncates the Ekitale Basin. The Ekitale Basin is then inverted [Colour figure can be viewed at wileyonlinelibrary.com]

temporal framework of the EARS. Then, the different stages of rift evolution in the northern Turkana Depression are described

(Figure 11), while discussing, in particular, factors controlling the structural evolution of the area.

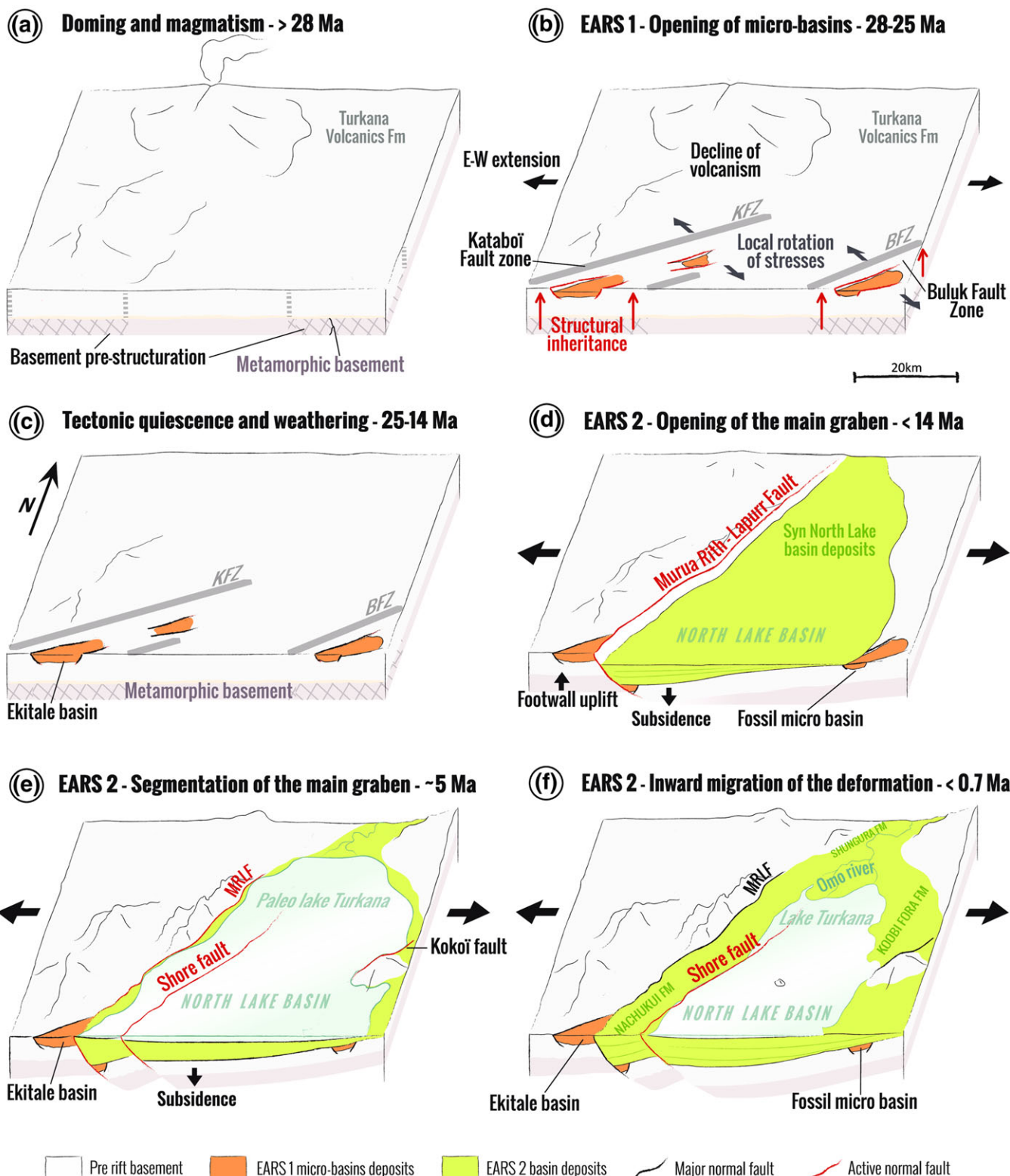


FIGURE 11 Scenario for the evolution of the Cenozoic EARS in the northern Turkana Depression. (a) Deposition of the extensive Turkana Volcanics Fm until 28 Ma precedes the first surface rupture in the area. (b) Early syn-rift micro-basins develop from a low differential stress that favoured the reactivation of oblique basement-inherited structures. (c) The first episode of rifting ends with a period of tectonic quiescence from ca. 25 to 14 Ma. (d) An increase of the differential stress and the extension rate lead to the opening of the North Lake Basin and the abandonment of non-optimal faults. (e) The main basin rift basin is then segmented into two main depocenters, ca. 5 Ma. (f) Up to the present day, the external depocenter has been inverted while deformation has migrated inward to the internal depocenter [Colour figure can be viewed at wileyonlinelibrary.com]

5.1 | Development of the Ekitale and the North Lake Basins within the regional chronological framework

Investigations of the Ekitale Basin show that its formation was initiated *ca.* 28 Ma and interrupted *ca.* 25.5 Ma. The Ekitale Basin represents the earliest evidence of surface rupture associated with the Cenozoic rifting in the northern Turkana Depression. Later, the extension was accommodated by initiation of the North Lake Basin to shape the current morphology of the northern Turkana Depression.

It is currently believed that the initial surface rupture associated with Cenozoic rifting in the northern Turkana Depression occurred *ca.* 15 Ma (Macgregor, 2015; Morley et al., 1999; Vétel & Le Gall, 2006) in the form of small-scale half-grabens (e.g., the Lapurr and Murua Rith basins). However, we show that the first extensional phase in the northern Turkana Depression is recorded by the Ekitale Basin, and that this phase occurred between 28 Ma and 25 Ma, some 13 Ma earlier than previously shown. Interestingly, the timing of this extensional phase matches with the Late Oligocene to Early Miocene rift climax in the Lokichar Basin, southern Turkana Depression, which is associated with the deposition of the Lokhone Shale (Macgregor, 2015; Morley et al., 1999). Previously, the Lokichar Basin was the only basin in the Turkana Depression associated with an Eocene–Oligocene extensional pulse, referred to as EARS 1 (Macgregor, 2015). The Ekitale Basin thus indicates that the extensional phase of EARS 1 also affected the northern Turkana Depression. Therefore, the EARS 1 extensional phase influenced a much larger area than previously depicted.

A second extensional phase (EARS 2, *sensu* Macgregor, 2015) marks the origin of most of the basins of the EARS. In the Turkana Depression, the onset of this second pulse was suspected to be diachronous, ranging from Upper Miocene in the southern Turkana Depression to Lower Pliocene in the northern Turkana Depression. In the northern Turkana Depression, this second pulse was thought to have begun between 9 and 4.2 Ma (Morley et al., 1999; Vétel & Le Gall, 2006) in association with the opening of the North Lake Basin. However, we show in this study that the North Lake Basin opened *ca.* 14 Ma, thus 5–10 Ma earlier than previously believed. Additionally, the Chew Bahir Basin (that constitutes the termination of the southern Main Ethiopian Rift, Figure 1b) opened *ca.* 20 Ma (Bonini et al., 2005; Pik, Marty, Carignan, Yirgu, & Ayalew, 2008), while the Southern Kerio Basin (northern termination of the Kenyan Rift Valley) began to form *ca.* 15 Ma (Torres Acosta et al., 2015). Considering these ages, a regional extensional pulse occurred over a ~6-Ma time interval within the northern Kenyan Rift Valley, the Turkana Depression, and the southern Main Ethiopian Rift. This pulse of extension is associated with EARS 2 (Macgregor, 2015), and its diachronicity is thus significantly reduced.

5.2 | Rifting in the northern Turkana Depression: Evolution of the controlling factors

The morphology of the Ekitale Basin is controlled by tectonic structures oriented broadly along a N50° direction, while more recent rift basins of the Turkana Depression, such as the North Lake Basin, are mainly organized along a N-S direction. The development of the

Ekitale Basin thus results from differing extensional conditions. Here, we propose a comprehensive model of the successive rifting phases from the pre-rift period to the modern configuration of the northern Turkana Depression. We discuss the nature of regional stresses that drove the development of the Ekitale Basin and the evolution of later rift basins.

Prior to 28 Ma, the area was affected by the deposition of the Turkana Volcanics Fm (Figure 11a). This volcanism resulted from the intense Late Eocene to mid-Miocene fissural volcanism activity (Bellieni et al., 1981; Bellieni et al., 1987; Walsh & Dodson, 1969; Zanettin et al., 1983). After 28 Ma, the EARS 1 pulse reactivated the basement-inherited NE–SW-oriented faults and led to the opening of the Ekitale Basin and other suspected comparable basins (Figure 11b). Reactivated faults were oriented N30°–50° and thus along a non-optimal direction regarding the E–W-oriented extension suggested at that time (Morley et al., 1999; Vétel & Le Gall, 2006). The opening of basins comparable to the Ekitale Basin, referred to as micro-basins, results from oblique rifting along the NW–SE direction. In addition, the reactivation of non-optimal faults requires less differential stress than that required to initiate failure of new optimal faults (Morley et al., 2004). This suggests that the oblique opening of the Ekitale Basin reflects a period during which both differential stress and the amount of extension were low. Thus, the initiation and morphology of the micro-basins are suspected to have been mainly driven by the ability of pre-existing inherited structures to be reactivated, while the opening of new structures was prevented by insufficient extension. The opening of these micro-basins contrasts with usual rift evolution models in which early syn-rift basins evolve within similar stress environments having a similar orientation (Gawthorpe & Leeder, 2000). This newly described syn-rift phase may be favoured during long-term rift evolution, separating pre-rift periods that experience no stress and the rift climax during which both differential stress and the amount of extension are high. Micro-basins comparable to the Ekitale Basin may develop during early-rift periods and may thus be characteristic of typical early-rift systems.

Following a period of tectonic quiescence between *ca.* 25 and *ca.* 14 Ma (Figure 11c), the EARS 2 extensional pulse opened the North Lake Basin in the northern Turkana Depression (Figure 11d). At *ca.* 14 Ma, the MRLF and other N–S-oriented structures, such as the minor faults and dykes, were initiated (Figure 11d). These truncated the Turkana Volcanics Fm and the Ekitale Basin. The remnant portion of the Ekitale Basin located on the newly formed rift shoulder was uplifted, leading to its inversion and abandonment. The newly formed North Lake Basin depocenter was controlled mainly by the activity of the MRLF. During this second extensional phase, previously active non-optimal N30°–50° faults were abandoned and optimal N–S-oriented faults developed. This transition from oblique to orthogonal rifting reflects the expression of a marked increase of σ_1 and thus an increase of the differential stress that focused the rupture along σ_2 (Morley et al., 2004). Thus, the amount of extension is believed to have been much greater during EARS 2 than during EARS 1 in the northern Turkana Depression.

After the opening of the North Lake Basin, several minor faults developed in the basin, parallel to the MRLF. One of them, the Shore Fault (Nutz et al., 2017), segmented the North Lake Basin into

external and internal sub-basins (Figure 11e). Although the timing of the segmentation remains unknown, seismic lines display wedging associated with the Shore Fault at least since 4.2–5 Ma, directly after the deposition of the Pliocene volcanics (Africa Oil Reports, 2016). Shortly thereafter, the Shore Fault became dominant in accommodating the extension. Around 0.7 Ma, the MRLF ceased to be active (Nutz et al., 2017). From this point, the main depocenter was associated with the Shore Fault while the external sub-basin was inverted (Figure 11f). This evolution marks the inward migration of the border fault, which is usually attributed to an increase in the amount of extension (Corti et al., 2010; Corti, Ranalli, Agostini, & Sokoutis, 2013).

The rift evolution in the northern Turkana Depression was largely driven by a progressive transition from a low to high regional differential stress and by a progressive increase in the amount of extension over time even if phases of extension were interrupted by periods of tectonic quiescence. The evolution of differential stress and the amount of extension could evolve in a broadly similar manner for other rift systems. Additionally, the identification of similar micro-basins related to an early-rift period in other rift systems could have wider implications, altering previously depicted timings of rift initiation and rifting history.

6 | CONCLUSIONS

The sedimentology and structures of the Ekitale Basin are documented through a detailed geological mapping, interpretation of five basin-scale sections and sedimentary facies analysis. The Ekitale Basin consists of a km-scale graben bounded by NE-SW-oriented normal faults. These normal faults originate from the reactivation, slightly after 28 Ma, of pre-existing basement-inherited structures. The sedimentary infill of the basin is referred to as the Topernawi Fm. From its base to top, it is composed of alluvial fan deltas and turbiditic complexes deposited in a lacustrine setting that are overlain by repeating pyroclastic deposits. The pyroclastic deposits are interbedded by fluvial deposits laid down during periods of volcanic quiescence. The evolution of the Ekitale Basin ceased ca. 25 Ma. Later, concomitant with the development of the North Lake Basin at ca. 14 Ma, N-S-oriented faults and dykes segmented the Ekitale Basin and led to its inversion. The Ekitale Basin is interpreted as a syn-rift basin associated with the first pulse of extension attributed to the Cenozoic rifting (EARS 1 sensu Macgregor, 2015). The Ekitale Basin characterizes the oldest expression of surface rupture associated with the Cenozoic rifting in the northern Turkana Depression. The opening of the Ekitale Basin originated from both a low amount of extension and a low differential stress that favoured the reactivation of non-optimal inherited faults during the early stages of Cenozoic rifting.

In the northern Turkana Depression, the Cenozoic rifting evolved through four main phases. Between 28 and 25 Ma, a first extensional pulse (EARS 1) was characterized by the development of non-optimal (regarding the E-W-oriented extension at that time) syn-rift basins, as the reactivation of pre-existing structures was the dominant control on basin morphology. Between 25 and 14 Ma, a relative tectonic quiescence led to the development of a significant weathering profile.

From 14 Ma, a second extensional pulse (EARS 2) produced a large N-S-oriented half-graben referred to as the North Lake Basin. It is attributed to the onset of the rift climax. The transition from oblique (EARS 1) to orthogonal (EARS 2) rifting is interpreted to reflect both a higher differential stress and a greater amount of extension. Finally, the North Lake Basin was segmented into two sub-basins prior to 4.2 Ma, while the resulting internal sub-basin became the only active depocenter after 0.7 Ma.

We present the first detailed evolution of the Cenozoic rifting in the northern Turkana Depression from the pre-rift settings to the modern configuration, refining the mode and timing of EARS 1 and EARS 2 phases in the area. A new phase in the rift evolution is documented, characterized by periods of low extension rate and low differential stresses. The identification of Ekitale-like syn-rift basins in other continental rift systems is the next step. Finally, this field-based investigation provides valuable new results for refining continental rift models.

ACKNOWLEDGEMENTS

This work was made possible thanks to a research grant from Total (Rift Lake Sedimentology—RiLakS research project; PI: MS) that provided postdoctoral funding to A. N. and a Master grant to T. R. We warmly thank Sonia Harmand-Lewis, Jason Lewis, and Sandrine Prat for sharing their remarkable camp facilities at Topernawi Laga, as well as all the members of the West Turkana Archeological Project. Satellite imagery (SPOT) was acquired at a special rate thanks to CNES/ISIS/Theia-Geosud. This work was conducted under a research permit attributed by NACOSTI. National Oil Corporation of Kenya (NOCK) is warmly thanked for their partnership (S. Hassan-Athmani, K. Nyagah, G. Muia, A. Karanja, and A. Ofafa). We are extremely grateful to our guides, Francis Emekwi Ekai and Sammy Lokorodi from Nariokotome. We thank Jackson Dongol for field assistance and James Ekitale for outstanding camp facilities. We thank the French Embassy in Kenya for help and support. J.-J. Tiercelin, M. Lescanne, M. Bez, and M. Diraison are warmly thanked for fruitful discussions. We deeply thank Marco Patacci, Xin Shan, and Steven Andrews for their constructive comments that helped improve the manuscript. We finally thank Murray Hay (Maxafeau Editing Services) for editing the English of the original manuscript.

ORCID

Théa Ragon  <http://orcid.org/0000-0002-1276-1910>

REFERENCES

- Abdelfettah, Y., Tiercelin, J.-J., Tarits, P., Hautot, S., Maia, M., & Thuo, P. (2016). Subsurface structure and stratigraphy of the northwest end of the Turkana Basin, Northern Kenya Rift, as revealed by magnetotellurics and gravity joint inversion. *Journal of African Earth Sciences*, 119(Supplement C), 120–138.
- Ackermann, R. V., Schlische, R. W., & Withjack, M. O. (2001). The geometric and statistical evolution of normal fault systems: An experimental study of the effects of mechanical layer thickness on scaling laws. *Journal of Structural Geology*, 23(11), 1803–1819.
- Africa Oil Reports (2016). Corporate presentations. Last retrieve May 4, 2017, from <http://www.africailcorp.com/s/presentations.asp>

- Alexander, J., Bridge, J., Cheel, R., & Leclair, S. (2001). Bedforms and associated sedimentary structures formed under supercritical water flows over aggrading sand beds. *Sedimentology*, 48(1), 133–152.
- Arambourg, C., & Wolff, R. (1969). Nouvelles données paléontologiques sur l'âge des gès du Lubur (Turkana grits) à l'Ouest du lac Rodolphe. *Comptes Rendus Société Géologique de France*, 6(1), 190–202.
- Ashley, G. M., Southard, J. B., & Boothroyd, J. C. (1982). Deposition of climbing-ripple beds: a flume simulation. *Sedimentology*, 29(1), 67–79.
- Bellieni, G., Visentin, E. J., Piccirillo, E., & Zanettin, B. (1987). Volcanic cycles and magmatic evolution in northern Turkana (Kenya). *Tectonophysics*, 143(1), 161–168.
- Bellieni, G., Visentin, E. J., Zanettin, B., Piccirillo, E., Di Brozolo, F. R., & Rita, F. (1981). Oligocene transitional tholeiitic magmatism in northern Turkana (Kenya): Comparison with the coeval Ethiopian volcanism. *Bulletin Volcanologique*, 44(3), 411–427.
- Bonini, M., Corti, G., Innocenti, F., Manetti, P., Mazzarini, F., Abebe, T., & Pecska, Z. (2005). Evolution of the main Ethiopian rift in the frame of Afar and Kenya rifts propagation. *Tectonics*, 24(1). TC1007
- Boone, S. C., Seiler, C., Kohn, B. P., Gleadow, A. J. W., Foster, D. A., & Chung, L. (2018). Influence of rift superposition on lithospheric response to East African Rift System extension: Lapur Range, Turkana, Kenya. *Tectonics*, 37(1). 2017TC004575
- Boschetto, H., Brown, F., & McDougall, I. (1992). Stratigraphy of the Lothidok Range, northern Kenya, and K/Ar ages of its Miocene primates. *Journal of Human Evolution*, 22(1), 47–71.
- Bosworth, W., Huchon, P., & McClay, K. (2005). The Red Sea and Gulf of Aden Basins. *Journal of African Earth Sciences*, 43(1), 334–378.
- Brown, F., & Feibel, C. (1991). Stratigraphy, depositional environments and palaeogeography of the Koobi Fora Formation. In J. M. Harris (Ed.), *Koobi Fora Research Project, vol.3, The fossil ungulates: Geology, fossil artiodactyls, and palaeoenvironments* (pp. 1–30). Oxford: Clarendon Press.
- Brown, F. H., & Fuller, C. R. (2008). Stratigraphy and tephra of the Kibish Formation, southwestern Ethiopia. *Journal of Human Evolution*, 55(3), 366–403.
- Bruhn, R. L., Brown, F. H., Gathogo, P. N., & Haileab, B. (2011). Pliocene volcano-tectonics and paleogeography of the Turkana Basin, Kenya and Ethiopia. *Journal of African Earth Sciences*, 59(2), 295–312.
- Brune, S., Corti, G., & Ranalli, G. (2017). Controls of inherited lithospheric heterogeneity on rift linkage: Numerical and analog models of interaction between the Kenyan and Ethiopian rifts across the Turkana depression. *Tectonics*, 36(9). 2017TC004739
- Buck, W. R. (1991). Modes of continental lithospheric extension. *Journal of Geophysical Research: Solid Earth*, 96(B12), 20161–20178.
- Butzer, K. W., & Thurber, D. L. (1969). Some Late Cenozoic sedimentary formations of the Lower Omo Basin. *Nature*, 222(5199), 1132–1143.
- Cartwright, J. A., Trudgill, B. D., & Mansfield, C. S. (1995). Fault growth by segment linkage: an explanation for scatter in maximum displacement and trace length data from the Canyonlands Grabens of SE Utah. *Journal of Structural Geology*, 17(9), 1319–1326.
- Cas, R., & Wright, J. (1988). *Volcanic successions modern and ancient: A geological approach to processes, products and successions*. Netherlands: Springer. 528 p
- Chorowicz, J. (2005). The East African Rift System. *Journal of African Earth Sciences*, 43(1), 379–410.
- Cole, P. D. (1991). Migration direction of sand-wave structures in pyroclastic-surge deposits: Implications for depositional processes. *Geology*, 19(11), 1108–1111.
- Corti, G., Ranalli, G., Agostini, A., & Sokoutis, D. (2013). Inward migration of faulting during continental rifting: Effects of pre-existing lithospheric structure and extension rate. *Tectonophysics*, 594(Supplement C), 137–148.
- Corti, G., Ranalli, G., Mulugeta, G., Agostini, A., Sani, F., & Zugu, A. (2010). Control of the rheological structure of the lithosphere on the inward migration of tectonic activity during continental rifting. *Tectonophysics*, 490(3), 165–172.
- Cowie, P. A. (1998). A healing-reloading feedback control on the growth rate of seismogenic faults. *Journal of Structural Geology*, 20(8), 1075–1087.
- Cowie, P. A., Gupta, S., & Dawers, N. H. (2000). Implications of fault array evolution for synrift depocentre development: Insights from a numerical fault growth model. *Basin Research*, 12(3–4), 241–261.
- Dawers, N. H., & Anders, M. H. (1995). Displacement-length scaling and fault linkage. *Journal of Structural Geology*, 17(5), 607–614.
- de Heinzelin, J. (1983). The Omo Group: Tervuren, Belgique, Musée Royal de l'Afrique Centrale, Annales, Série in 8°Sciences Géologiques, 85, 241–303.
- Ducrocq, S., Boissarie, J. R., Tiercelin, J. J., Delmer, C., Garcia, G., Kyalo, M. F., ... Lihoreau, F. (2010). New Oligocene vertebrate localities from Northern Kenya (Turkana basin). *Journal of Vertebrate Paleontology*, 30(1), 293–299.
- Duller, R. A., Mountney, N. P., Russell, A. J., & Cassidy, N. C. (2008). Architectural analysis of a volcaniclastic jökulhlaup deposit, southern Iceland: Sedimentary evidence for supercritical flow. *Sedimentology*, 55(4), 939–964.
- Dunkelman, T. J., Karson, J. A., & Rosendahl, B. R. (1988). Structural style of the Turkana rift, Kenya. *Geology*, 16(3), 258–261.
- Dunkelman, T. J., Rosendahl, B. R., & Karson, J. A. (1989). Structure and stratigraphy of the Turkana rift from seismic reflection data. *Journal of African Earth Sciences (and the Middle East)*, 8(2), 489–510.
- Ebinger, C. J., & Sleep, N. H. (1998). Cenozoic magmatism throughout East Africa resulting from impact of a single plume. *Nature*, 395(6704), 788–791.
- Ebinger, C. J., Yemane, T., Harding, D. J., Tesfaye, S., Kelley, S., & Rex, D. C. (2000). Rift deflection, migration, and propagation: Linkage of the Ethiopian and Eastern rifts, Africa. *Geological Society of America Bulletin*, 112(2), 163–176.
- Feibel, C. S. (2003). Stratigraphy and depositional history of the Lothagam sequence. In M. G. Leakey and J. M. Harris (eds.), *Lothagam: The dawn of humanity in Eastern Africa*, M. G. Leakey and J. M. Harris (pp. 17–29). Columbia University Press, New York.
- Feibel, C. S. (2011). A geological history of the Turkana Basin. *Evolutionary Anthropology: Issues, News, and Reviews*, 20(6), 206–216.
- Fielding, C. R. (2006). Upper flow regime sheets, lenses and scour fills: Extending the range of architectural elements for fluvial sediment bodies. *Sedimentary Geology*, 190(1), 227–240.
- Fisher, R. V. (1961). Proposed classification of volcaniclastic sediments and rocks. *Geological Society of America Bulletin*, 72(9), 1409–1414.
- Fisher, R. V., & Schmincke, H. U. (1984). *Pyroclastic rocks*. Berlin: Springer. 472 pp
- Fossen, H., & Rotevatn, A. (2016). Fault linkage and relay structures in extensional settings—A review. *Earth-Science Reviews*, 154, 14–28.
- Furman, T., Bryce, J. G., Karson, J., & Iotti, A. (2004). East African Rift System (EARS) plume structure: Insights from Quaternary Mafic Lavas of Turkana, Kenya. *Journal of Petrology*, 45(5), 1069–1088.
- Furman, T., Kaleta, K. M., Bryce, J. G., & Hanan, B. B. (2006). Tertiary mafic lavas of Turkana, Kenya: Constraints on East African plume structure and the occurrence of high- μ volcanism in Africa. *Journal of Petrology*, 47(6), 1221–1244.
- Gathogo, P. N., & Brown, F. H. (2006). Stratigraphy of the Koobi Fora Formation (Pliocene and Pleistocene) in the Illel region of northern Kenya. *Journal of African Earth Sciences*, 45(4), 369–390.
- Gathogo, P. N., Brown, F. H., & McDougall, I. (2008). Stratigraphy of the Koobi Fora Formation (Pliocene and Pleistocene) in the Loiyangalani region of northern Kenya. *Journal of African Earth Sciences*, 51(5), 277–297.
- Gawthorpe, R., & Leeder, M. (2000). Tectono-sedimentary evolution of active extensional basins. *Basin Research*, 12(3–4), 195–218.

- Gilbert, J. S., & Lane, S. J. (1994). The origin of accretionary lapilli. *Bulletin of Volcanology*, 56(5), 398–411.
- Gregory, J. W. (1896). *The Great Rift Valley: Being the narrative of a journey to Mount Kenya and Lake Baringo: With some account of the geology, natural history, anthropology and future prospects of British East Africa* (p. 422). London, United Kingdom: John Murray.
- Gupta, S., Cowie, P. A., Dawers, N. H., & Underhill, J. R. (1998). A mechanism to explain rift-basin subsidence and stratigraphic patterns through fault-array evolution. *Geology*, 26(7), 595–598.
- Harris, J. M., Leakey, M. G., & Brown, F. H. (1988). Stratigraphy and paleontology of Pliocene and Pleistocene localities west of Lake Turkana, Kenya. Natural History Museum of Los Angeles County.
- Hart, B. S., & Plint, A. G. (1995). Gravelly shoreface and beachface deposits. In A. G. Plint (Ed.), *Sedimentary facies analysis* (pp. 75–99). Hoboken, NJ: Blackwell Publishing Ltd.
- Hendrie, D., Kusznir, N., Morley, C., & Ebinger, C. (1994). Cenozoic extension in northern Kenya: A quantitative model of rift basin development in the Turkana region. *Tectonophysics*, 236(1), 409–438.
- Jicha, B. R., & Brown, F. H. (2014). An age for the Korath Range, Ethiopia and the viability of 40 Ar/39 Ar dating of kaersutite in Late Pleistocene volcanics. *Quaternary Geochronology*, 21, 53–57.
- Jobe, Z. R., Lowe, D. R., & Morris, W. R. (2012). Climbing-ripple successions in turbidite systems: Depositional environments, sedimentation rates and accumulation times. *Sedimentology*, 59(3), 867–898.
- Kneller, B. (2003). The influence of flow parameters on turbidite slope channel architecture. *Marine and Petroleum Geology*, 20(6–8), 901–910.
- Macdonald, G. A. (1953). Pahoehoe, aa, and block lava. *American Journal of Science*, 251(3), 169–191.
- Macgregor, D. (2015). History of the development of the East African Rift System: A series of interpreted maps through time. *Journal of African Earth Sciences*, 101, 232–252.
- Mansfield, C., & Cartwright, J. (2001). Fault growth by linkage: Observations and implications from analogue models. *Journal of Structural Geology*, 23(5), 745–763.
- McDougall, I., & Brown, F. H. (2009). Timing of volcanism and evolution of the northern Kenya Rift. *Geological Magazine*, 146(01), 34–47.
- McDougall, I., & Feibel, C. S. (1999). Numerical age control for the Miocene-Pliocene succession at Lothagam, a hominoid-bearing sequence in the northern Kenya Rift. *Journal of the Geological Society*, 156(4), 731–745.
- Moorhouse, B. L., & White, J. D. L. (2016). Interpreting ambiguous bedforms to distinguish subaerial base surge from subaqueous density current deposits. *The Depositional Record*, 2(2), 173–195.
- Morley, C. (1994). Interaction of deep and shallow processes in the evolution of the Kenya rift. *Tectonophysics*, 236(1), 81–91.
- Morley, C. (1999). Basin evolution trends in East Africa. In C. K. Morley (Ed.), *Geoscience of rift systems: Evolution of East Africa*. American Association of Petroleum Geologists Studies in Geology, No. 44. (pp. 131–150).
- Morley, C., Karanja, F., Wescott, W., Stone, D., Harper, R., Wigger, S., & Day, R. (1999). Geology and geophysics of the Western Turkana Basins, Kenya. In C. K. Morley (Ed.), *Geoscience of rift systems: Evolution of East Africa*. American Association of Petroleum Geologists Studies in Geology, No. 44. (pp. 19–54).
- Morley, C. K., Haranya, C., Phoosongsee, W., Pongwapee, S., Kornsawan, A., & Wonganan, N. (2004). Activation of rift oblique and rift parallel pre-existing fabrics during extension and their effect on deformation style: Examples from the rifts of Thailand. *Journal of Structural Geology*, 26(10), 1803–1829.
- Morley, C. K., Wescott, W., Stone, D., Harper, R., Wigger, S., & Karanja, F. (1992). Tectonic evolution of the northern Kenyan Rift. *Journal of the Geological Society*, 149(3), 333–348.
- Muiia, G. (2015). *The Turkana Grits: Potential hydrocarbon reservoirs of the Northern and Central Kenya Rifts*. PhD thesis, Université de Rennes, France, 202p.
- Mulder, T., & Alexander, J. (2001). The physical character of subaqueous sedimentary density flows and their deposits. *Sedimentology*, 48(2), 269–299.
- Mulder, T., Migeon, S., Savoye, B., & Faugères, J. C. (2001). Inversely graded turbidite sequences in the deep Mediterranean: a record of deposits from flood-generated turbidity currents? *Geo-Marine Letters*, 21(2), 86–93.
- Mulder, T., Syvitski, J. P. M., Migeon, S., Faugères, J.-C., & Savoye, B. (2003). Marine hyperpycnal flows: Initiation, behavior and related deposits. A review. *Marine and Petroleum Geology*, 20(6), 861–882.
- Mutti, E., Tinterri, R., Benevelli, G., di Biase, D., & Cavanna, G. (2003). Deltaic, mixed and turbidite sedimentation of ancient foreland basins. *Marine and Petroleum Geology*, 20(6–8), 733–755.
- Nutz, A., Schuster, M., Boës, X., & Rubino, J.-L. (2017). Orbitally-driven evolution of Lake Turkana (Turkana Depression, Kenya, EARS) between 1.95 and 1.72 Ma: A sequence stratigraphy perspective. *Journal of African Earth Sciences*, 125, 230–243.
- Nutz, A., Schuster, M., Ghienne, J.-F., Roquin, C., & Bouchette, F. (2018). Wind-driven waterbodies: A new category of lake within an alternative sedimentologically-based lake classification. *Journal of Paleolimnology*, 59(2), 189–199.
- Owen, G. (1996). Experimental soft-sediment deformation: Structures formed by the liquefaction of unconsolidated sands and some ancient examples. *Sedimentology*, 43(2), 279–293.
- Owen, G., & Moretti, M. (2011). Identifying triggers for liquefaction-induced soft-sediment deformation in sands. *Sedimentary Geology*, 235(3), 141–147.
- Owen, R. B., Barthelme, J. W., Renaut, R. W., & Vincens, A. (1982). Palaeolimnology and archaeology of Holocene deposits north-east of Lake Turkana, Kenya. *Nature*, 298, 523–529.
- Pettijohn, F. J., Potter, P. E., & Siever, R. (2012). *Sand and sandstone*. New York: Springer-Verlag. 553 p
- Pik, R., Marty, B., Carignan, J., Yirgu, G., & Ayalew, T. (2008). Timing of East African Rift development in southern Ethiopia: Implication for mantle plume activity and evolution of topography. *Geology*, 36(2), 167–170.
- Postma, G. (1990). Depositional architecture and facies of river and fan deltas: a synthesis. In A. Colella, & D. B. Prior (Eds.), *Coarse-grained deltas: International Association of Sedimentologists Special Publication*, 10 (pp. 13–27).
- Prosser, S. (1993). Rift-related linked depositional systems and their seismic expression. *Geological Society, London, Special Publications*, 71(1), 35–66.
- Renne, P. R., Mundil, R., Balco, G., Min, K., & Ludwig, K. R. (2010). Joint determination of 40K decay constants and 40Ar*/40K for the Fish Canyon sanidine standard, and improved accuracy for 40Ar/39Ar geochronology. *Geochimica et Cosmochimica Acta*, 74(18), 5349–5367.
- Renne, P. R., Swisher, C. C., Deino, A. L., Karner, D. B., Owens, T. L., & DePaolo, D. J. (1998). Intercalibration of standards, absolute ages and uncertainties in 40Ar/39Ar dating. *Chemical Geology*, 145(1), 117–152.
- Rooney, T. O., Herzberg, C., & Bastow, I. D. (2012). Elevated mantle temperature beneath East Africa. *Geology*, 40(1), 27–30.
- Rosendahl, B. R. (1987). Architecture of continental rifts with special reference to East Africa. *Annual Review of Earth and Planetary Sciences*, 15, 445–503.
- Ruffet, G., Féraud, G., & Amouric, M. (1991). Comparison of 40Ar-39Ar conventional and laser dating of biotites from the North Trégor Batholith. *Geochimica et Cosmochimica Acta*, 55(6), 1675–1688.
- Ruffet, G., Féraud, G., Balèvre, M., & Kiéna, J.-R. (1995). Plateau ages and excess argon in phengites: An 40Ar/39Ar laser probe study of Alpine micas (Sesia Zone, Western Alps, northern Italy). *Chemical Geology*, 121(1), 327–343.
- Schmincke, H.-U., Fisher, R. V., & Waters, A. C. (1973). Antidune and chute and pool structures in the base surge deposits of the Laacher See area, Germany. *Sedimentology*, 20(4), 553–574.

- Simon, B., Guillocheau, F., Robin, C., Dauteuil, O., Nalpas, T., Pickford, M., ... Bez, M. (2017). Deformation and sedimentary evolution of the Lake Albert Rift (Uganda, East African Rift System). *Marine and Petroleum Geology*, 86(Supplement C), 17–37.
- Smith, R. L. (1960). Ash Flows. *Geological Society of America Bulletin*, 71(6), 795–841.
- Talling, P. J., Masson, D. G., Sumner, E. J., & Malgesini, G. (2012). Subaqueous sediment density flows: Depositional processes and deposit types. *Sedimentology*, 59(7), 1937–2003.
- Thuo, P. (2009). *Stratigraphic, petrographic and diagenetic evaluation of Cretaceous/Paleogene potential reservoir sandstones of Western Turkana, Kenya. Implications on the petroleum potential of Northwestern Kenya*. PhD thesis, Université de Bretagne, Occidentale, Brest, France, 139 p.
- Tiercelin, J.-J., & Lezzar, K.-E. (2002). A 300 million years history of rift lakes in Central and East Africa: An updated broad review. In E. O. Odada, & D. O. Ologo (Eds.), *The East African Great Lakes: Limnology, palaeolimnology and biodiversity* (pp. 3–60). Springer Netherlands.
- Tiercelin, J.-J., Potdevin, J.-L., Morley, C., Talbot, M., Bellon, H., Rio, A., ... Vétel, W. (2004). Hydrocarbon potential of the Meso-Cenozoic Turkana Depression, northern Kenya. I. Reservoirs: Depositional environments, diagenetic characteristics, and source rock-reservoir relationships. *Marine and Petroleum Geology*, 21(1), 41–62.
- Tiercelin, J.-J., Potdevin, J.-L., Thuo, P. K., Abdelfettah, Y., Schuster, M., Bourquin, S., ... Ruffet, G. (2012). Stratigraphy, sedimentology and diagenetic evolution of the Lapur sandstone in northern Kenya: Implications for oil exploration of the Meso-Cenozoic Turkana depression. *Journal of African Earth Sciences*, 71–72(Supplement C), 43–79.
- Tiercelin, J.-J., Schuster, M., Roche, H., Brugal, J.-P., Thuo, P., Prat, S., ... Bohn, M. (2010). New considerations on the stratigraphy and environmental context of the oldest (2.34 Ma) Lokalalei archaeological site complex of the Nachukui Formation, West Turkana, northern Kenya Rift. *Journal of African Earth Sciences*, 58(2), 157–184.
- Tiercelin, J.-J., Thuo, P. K., Potdevin, J.-L., & Nalpas, T. (2012). Hydrocarbon prospectivity in Mesozoic and Early-Middle Cenozoic Rift Basins of Central and Northern Kenya, Eastern Africa. In D. Gao (Ed.), *Tectonics and sedimentation: Implications for petroleum systems: American Association of Petroleum Geologists Memoir 100* (pp. 179–207).
- Torres Acosta, V., Bande, A., Sobel, E. R., Parra, M., Schildgen, T. F., Stuart, F., & Strecker, M. R. (2015). Cenozoic extension in the Kenya Rift from low-temperature thermochronology: Links to diachronous spatiotemporal evolution of rifting in East Africa. *Tectonics*, 34(12), 2015TC003949.
- Vétel, W. (2005). *Dynamique de l'extension intra-continentale en contexte de rift magmatique: le Rift Turkana (Nord Kenya) de l'Eocène à l'Actuel*. Ph.D. Thesis, Université de Bretagne occidentale-Brest. Retrieved from <http://tel.archives-ouvertes.fr/tel-00009294/>.
- Vétel, W., & Le Gall, B. (2006). Dynamics of prolonged continental extension in magmatic rifts: The Turkana Rift case study (North Kenya). *Geological Society, London, Special Publications*, 259(1), 209–233.
- Walker, G. P. (1984). Characteristics of dune-bedded pyroclastic surge bedsets. *Journal of Volcanology and Geothermal Research*, 20(3), 281–296.
- Walsh, J., and Dodson, R. G. (1969). Geology of Northern Turkana. *Geological Survey of Kenya*.
- Waters, A. C., & Fisher, R. V. (1971). Base surges and their deposits: Capelinhos and Taal volcanoes. *Journal of Geophysical Research*, 76(23), 5596–5614.
- Wescott, W., Morley, C., & Karanja, F. (1993). Geology of the Turkana Grits in the Lariu range and Mt. Porr areas, southern Lake Turkana, north-western Kenya. *Journal of African Earth Sciences (and the Middle East)*, 16(4), 425–435.
- Whipp, P. S., Jackson, C. L., Schlische, R. W., Withjack, M. O., & Gawthorpe, R. L. (2016). Spatial distribution and evolution of fault-segment boundary types in rift systems: Observations from experimental clay models. *Geological Society, London, Special Publications*, 439(1), 79–107.
- Williamson, P. G., & Savage, R. J. (1986). Early rift sedimentation in the Turkana basin, northern Kenya. *Geological Society, London, Special Publications*, 25(1), 267–283.
- Wilson, C. J. N., & Walker, G. P. L. (1982). Ignimbrite depositional facies: The anatomy of a pyroclastic flow. *Journal of the Geological Society*, 139(5), 581–592.
- Wohletz, K. H., & Sheridan, M. F. (1979). A model of pyroclastic surge. *Geological Society of America Special Papers*, 180, 177–194.
- Wright, L. D. (1977). Sediment transport and deposition at river mouths: A synthesis. *Geological Society of America Bulletin*, 88(6), 857–868.
- Zanettin, B., Justin Visentin, E., Bellieni, G., Piccirillo, E., & Rita, F. (1983). Le volcanisme du Bassin du Nord-Turkana (Kenya): Age, succession et évolution structurale. In *Rifts et Fossés Anciens* (ed., Vol. 7). *Bulletin Des Centres de Recherches Exploration-Production Elf-Aquitaine*. (pp. 249–255).
- Zavala, C., Arcuri, M., Meglio, M. D., Diaz, H. G., & Contreras, C. (2011). A genetic facies tract for the analysis of sustained hyperpycnal flow deposits. In R. M. Slatt, & C. Zavala (Eds.), *Sediment transfer from shelf to deep water—Revisiting the delivery system*. *American Association of Petroleum Geologists Studies in Geology No. 61*. (pp. 31–51).
- Zavala, C., Arcuri, M., & Valiente, L. (2012). The importance of plant remains as diagnostic criteria for the recognition of ancient hyperpycnites. *Revue de Paléobiologie*, 11, 457–469.

SUPPORTING INFORMATION

Additional supporting information may be found online in the Supporting Information section at the end of the article.

How to cite this article: Ragon T, Nutz A, Schuster M, Ghienne J-F, Ruffet G, Rubino J-L. Evolution of the northern Turkana Depression (East African Rift System, Kenya) during the Cenozoic rifting: New insights from the Ekitale Basin (28–25.5 Ma). *Geological Journal*. 2018;1–21. <https://doi.org/10.1002/gj.3339>